Quantitative study of 3D and 2D strong localization of matter waves by atomic scatterers

Mauro Antezza, Yvan Castin, David Hutchinson

Quantitative study of 3D and 2D strong localization of matter waves by atomic scatterers

Mauro Antezza and Yvan Castin
Laboratoire Kastler Brossel, École Normale Supérieure, CNRS and UPMC, 24 rue Lhomond, 75231 Paris, France

David A. W. Hutchinson
The Jack Dodd Centre for Quantum Technology, Department of Physics, University of Otago, Dunedin 9016, New Zealand

(Dated: June 22, 2010)

We study the strong localization of atomic matter waves in a disordered potential created by atoms pinned at the nodes of a lattice, for both 3D and 2D systems. The localization length of the matter wave, the density of localized states, and the occurrence of energy mobility edges (for the 3D system), are numerically investigated as a function of the effective scattering length between the atomic matter wave and the pinned atoms. Both positive and negative matter wave energies are explored. Interesting features of the density of states are discovered at negative energies, where maximums in the density of bound states for the system can be interpreted in terms of bound states of a matter wave atom with a few pinned atomic scatterers. In 3D we found evidences of up to three mobility edges, one at positive energies, and two at negative energies, the latter corresponding to transitions between extended and localized bound states. In 2D, no mobility edge is found, and a rapid exponential-like increase of the localization length is observed at high energy.

PACS numbers: 67.85.-d,67.10.Jn,71.23.An
Keywords:

I. INTRODUCTION

Propagation of waves in disordered systems is a rich physical phenomenon, object of enduring research interest. Its complexity is due to the fact that the scattering of a wave by a random potential depends on several features: energy and type of the wave, internal and external degrees of freedom of the scattering potential, dimensionality and symmetry of the physical system, and possible presence of interaction among the propagating waves. Such variety is the reason of a wide experimental and theoretical studies of the diffusion of several kind of classical and quantum waves by many kinds of disordered potentials. This field of research was started by P.W. Anderson [1], who predicted in 3D the localization of a quantum particle experiencing short range hoping between discrete sites, when the on-site energies are sufficiently random. Several theories have been developed, leading to a general consensus on the fact that a wave is localized in 1D and 2D infinite disordered systems, independently of its energy and of the strength of disorder. In 3D systems a metal-insulator phase transition induced by sufficiently strong disorder may take place: it exists one (or more) critical energy E_c (called the mobility edge) which separates two energy regions. Waves with an energy on one side of E_c are spatially localized (transport is absent), while waves with an energy on the other side are extended over the entire space (transport is diffusive). The localized waves are characterized by an amplitude which decrease exponentially in space at large distances from a central region, defining a typical length, called the *localization length* ξ. The richness of the phase transition appears in the critical region around the critical energy E_c: here the physics is supposed to be universal, depending only on the symmetries of the system, and not explicitly on the kind of wave or disordered potential. This is due to the fact that, in the critical region, the localization length diverges with a power low behavior $\xi \propto |E - E_c|^\nu$, where the critical exponent ν characterizes the universality class of the phase transition [17–19].

The localization of waves appears as a very rich phenomenon, but it is also very delicate and complex, often difficult to observe experimentally due to parasitic effects (absorption of the wave, finite size effects, ...). A large scientific literature exists on the wave localization for several physical systems. Here we deal with the localization of ultra-cold atomic matter waves. Indeed, ultra-cold atomic gases offer a unique system in terms of isolation from environment, cleanness of the system, realization of the system in several spatial dimensions (1D, 2D, 3D), development of several direct detection techniques, and control of the interaction strength. One can even imagine localizing different kinds of waves (matter or light) in different kinds of disordered potentials (created by light or matter). Recently, several experimental investigations on the localization of atomic matter waves have been performed: in a 1D genuine disordered potential made by a laser speckle [2], in a 1D bi-chromatic optical lattice (strictly speaking, this is not true disorder, but it is possible to observe a localization-delocalization transition) [3], and in an atomic quasi-periodic kicked rotor where a localization in momentum space has been reported (true disorder again is absent, but the system, which is 1D in

real space, can be mapped into an Anderson model with several effective dimensions in momentum space, giving the possibility to extract the critical exponents of a 3D Anderson transition) [4].

A different way to realize a disordered potential for atomic matter waves, using atoms pinned at random positions at the nodes of an optical lattice, was proposed in [5]. This proposal has potentially several advantages over the laser speckle route. On the experimental side, it can be realized as easily in 1D, in 2D, and in 3D, and also since an optimization of the matter wave interaction with each individual scatterer may be performed, one may hope to reach very short mean free paths and localization lengths. On the theoretical side, it allows an exact numerical study for a large number of scatterers - as many as in typical experiments as we shall see. A quantitative study of this model was done for a 1D system [5], predicting minimal localization lengths $\lesssim 10\mu$m. A first investigation of the model for 3D systems was performed in [6], revealing the existence of a large density of localized states with a very short localization length (a few microns) for positive energies. Recently, similar models have been considered in the case where the matter wave experiences both a periodic potential and interactions among the A atoms [7].

In this paper, we study more extensively the behavior of the matter wave localization for this model, for both 3D and 2D systems, for both positive and negative energies, and for a broad range of values of the matter wave-pinned atom interaction strength. We explicitly study the features of the localization length and of the density of localized states, the occurrence of mobility edges, and the effect of the presence of an underlying periodic lattice. We find that, both in 2D and 3D, a strongly resonant interaction between the matter wave and each pinned atom is required to obtain localized states with small localization lengths. On the experimental side, this requires a tuning of this interaction by use of a Feshbach resonance. First steps in this direction were recently taken: confinement induced resonances between almost free $A = {}^{87}$Rb atoms and $B = {}^{41}$K atoms tightly trapped in a 1D laser standing wave were observed [14].

The article is organized as follows. The first part deals with the 3D case: We present the model in section II, we calculate the localization length in section III by studying the response of the system to a source in the medium, we calculate and discuss the density of localized states in section IV, in the form of resonances at positive energies and bound states at negative energies. The second part of the article contains the same analysis for the 2D case, see section V. We conclude in section VI.

II. PHYSICAL SYSTEM AND MODEL

We consider two atomic species, A and B. The B atoms are tightly trapped at the nodes of a cubic optical lattice of lattice spacing d, in a regime where their tunneling among the neighboring lattice sites is negligible over the duration of the experiment. These B atoms are prepared in the vibrational ground state of the local microtrap, and are randomly distributed among the lattice sites, with a uniform occupation probability $p_{\rm occ}$ inside a sphere of radius R; their locations are independent random variables, except for the constraint that there is nowhere more than one B atom per lattice site.

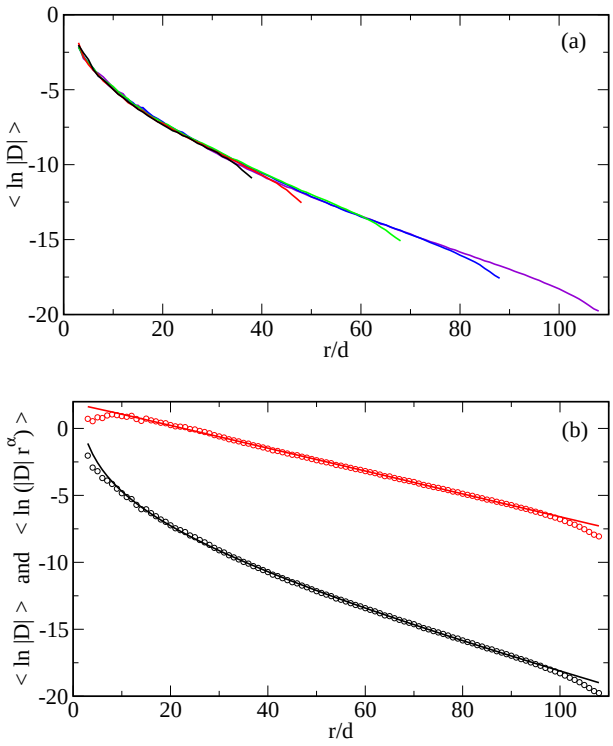

FIG. 1: For a source placed at the origin $\mathbf{r}_0 = \mathbf{0}$, coarse grained histogram giving $\langle \ln |D| \rangle$ as a function of the distance from the source, averaged over 100 realizations of disorder. The lattice for the B atoms is cubic with a lattice constant d, and a filling factor $p_{\rm occ} = 1/10$. The energy of the emitting source is $E = \hbar^2 k^2/2m$ with $kd = 0.94$. The effective scattering length is $a_{\rm eff} = 0.7d$. (a) Coarse grained histogram for 5 different radii R of the sphere containing the scatterers: $R/d = 40$ (black), $R/d = 50$ (red), $R/d = 70$ (green), $R/d = 90$ (blue), $R/d = 110$ (violet). (b) For $R/d = 110$, coarse grained histogram (black circles) and its fit by the functional form Eq. (10) (black solid line), resulting in $\kappa d = 0.086$ and $\alpha = 2.5$; the same histogram (red circles) and the same fit (red solid line) with D_i multiplied by r_i^α. The fit was performed over the interval $10 < r/d < 90$. Note that the largest considered value of $R/d = 110$ corresponds to a number of scatterers $N \simeq 5.6 \times 10^5$.

The A atoms form the matter wave to be strongly localized. They are assumed to move freely in space (in particular they are insensitive to the optical lattice), except that they scatter on the B atoms. This scattering is assumed to be elastic, under the condition that the kinetic energy of the A atoms is much smaller than the quantum of oscillation of the trapped B atoms, $\frac{\hbar^2 k^2}{2m} \ll \hbar\omega_{\rm osc}$,

where m and $\hbar k$ are the mass and momentum of an A atom. This scattering is also assumed to be in the zero-range regime $ka_{\rm ho} \ll 1$ where the $a_{\rm ho}$ is the harmonic oscillator length of the B atoms. In this case, the B atoms may be considered as point-like scatterers, and the $A-B$ scattering is characterized by the effective scattering length $a_{\rm eff}$ [29]. Remarkably, using a Feshbach resonance technique to adjust the free-space $A-B$ scattering length a, one can realize confinement-induced resonances leading to arbitrarily large values of $a_{\rm eff}$ [6]. The B atoms may thus effectively constitute a static and strong disordered potential for the matter wave.

The problem is thus modeled as follows: The matter wave Hamiltonian is that of the free A atom, $\mathcal{H} = -\frac{\hbar^2}{2m}\Delta_{\mathbf{r}}$, with the $A-B$ interaction replaced by the following contact conditions for the matter wave wavefunction $\psi(\mathbf{r})$: there exist complex numbers D_i such that

$$\psi(\mathbf{r}) = -\frac{m}{2\pi\hbar^2}\, D_i \left[|\mathbf{r}-\mathbf{r}_i|^{-1} - a_{\rm eff}^{-1}\right] + O(|\mathbf{r}-\mathbf{r}_i|) \quad (1)$$

in the vicinity of each B scatterer location $\mathbf{r}_i$. The factor $m/(2\pi\hbar^2)$ is introduced for convenience. The Bethe-Peierls contact condition (1) is equivalent to the pseudo-potential as used in [6].

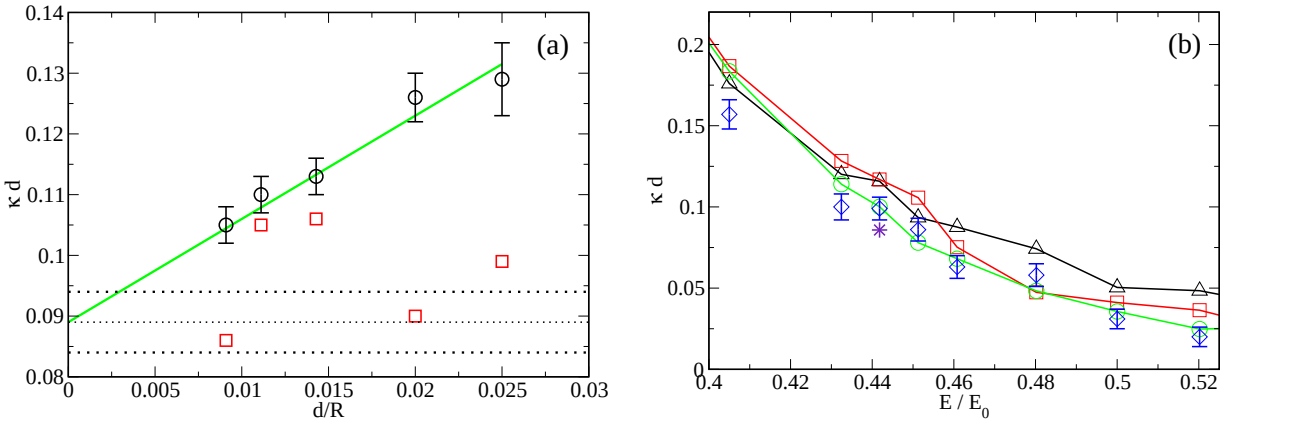

FIG. 2: For the 3D system: Comparison of the two methods of calculating the Lyapunov exponent $\kappa = 1/\xi$. As in Fig.1, the filling factor is $p_{\rm occ} = 1/10$, and the effective scattering length is $a_{\rm eff} = 0.7d$. (a) Lyapunov exponent κ for a fixed energy of the emitting source, $E = \hbar^2k^2/2m$ with $kd = 0.94$. Red squares: Lyapunov exponent from the first method, see Eq. (10), for several values of d/R; each point is the result of a fitting on the interval $10d < r < R - 20d$. The second method, see Eqs. (13), (14), and (15), leads to a Lyapunov exponent which is the extrapolation at $d/R = 0$ of the black circles; the green straight solid line is the linear extrapolation, giving $\kappa d = 0.089 \pm 0.005$ at $d/R = 0$; the three horizontal dotted lines represent the value of κ and its confidence interval. The two methods are essentially compatible if one considers the scatter in the data for the first method and the error bars for the second one. (b) For the two methods, Lyapunov exponent κ as a function of energy of the emitting source $E = \hbar^2k^2/2m$. The lattice spacing d of the cubic lattice, and the energy $E_0 = \hbar^2/(md^2)$, are used as units. Note that $E_0 = 2E_{\rm rec}/\pi^2$, where $E_{\rm rec}$ is the atomic recoil energy after absorption of a lattice photon. Here the filling factor is $p_{\rm occ} = 1/10$, and the effective scattering length is $a_{\rm eff} = 0.7d$. The solid lines and the violet star are obtained with the first method [see Eq. (10)]. The three solid lines correspond to sphere radius $R = 50d$ (black line, triangles), $R = 60d$ (red line, squares), $R = 70d$ (green line, circles), and an average over 500 realizations of disorder. The violet star corresponds to a bigger sphere with radius $R = 110d$, and 100 realizations of disorder. The blue diamond symbols with error bars, are obtained with the second method [see Eqs. (13), (14), and (15)] where the extrapolation has been performed using $d/R = 1/50$, $d/R = 1/60$, $d/R = 1/70$, and 500 realizations of disorder. The second method provides results essentially in agreement with those of the first method. Note the quite small values of the Lyapunov exponents (large localization lengths).

Here, the disordered potential has a finite extension, so that all the positive energy eigenstates are extended states belonging to a continuum. However, the localized states that would exist for a strictly infinite extension disorder have *precursors* in the form of sharp resonances with a width tending exponentially to zero with the disorder extension [6, 12]. At negative energies the matter wave is bound inside the gas of scatterers, and the corresponding bound states can be either extended or localized. The appropriate tool to find these resonances and bound states is the matter wave Green's function for an energy E, for a *given* realization of the disorder,

$$G(\mathbf{r},\mathbf{r}') = \langle \mathbf{r}| \left(\frac{1}{E + i0^+ - \mathcal{H}}\right)_{\rm c.c.} |\mathbf{r}'\rangle \quad (2)$$

and its analytical continuation to complex energies in the

lower half-plane. Note that $G(\mathbf{r},\mathbf{r}')$ is subject to the same contact conditions as ψ in (1), hence the subscript c.c. in Eq.(2). This Green's function G actually plays a major role in the theory of transport phenomena: The large $|\mathbf{r}-\mathbf{r}'|$ behaviors of $\langle G(\mathbf{r},\mathbf{r}')\rangle$ and $\langle \ln|G(\mathbf{r},\mathbf{r}')|\rangle$ provide the scattering mean free path and the localization length, respectively, where $\langle\ldots\rangle$ represents the average over all realizations of disorder, that is over the B locations.

A remarkable feature of the point-like scatterers is that the Green's function may be obtained by the solution of a $N\times N$ complex linear system, where N is the number of B scatterers. This allows an exact numerical calculation, up to $N\approx 10^5$ in this work, a value of the order of typical experiments with atoms in optical lattices.

This remarkable feature may be derived as follows. One starts with the fact that the Green's function $G(\mathbf{r},\mathbf{r}_0)$ obeys a Schrödinger equation with a point-like source term $\delta(\mathbf{r}-\mathbf{r}_0)$ of matter waves at position $\mathbf{r}_0$. The diverging terms of the contact conditions (1) for the Green's function give rise to secondary point-like sources of amplitudes D_i at the scatterers' positions $\mathbf{r}_i$, by virtue of the usual relation $\Delta_{\mathbf{r}}|\mathbf{r}-\mathbf{r}_i|^{-1}=-4\pi\delta(\mathbf{r}-\mathbf{r}_i)$. The resulting wave equation is thus

$$\left(E+i0^+ +\frac{\hbar^2}{2m}\Delta_{\mathbf{r}}\right)G(\mathbf{r},\mathbf{r}_0)=\delta(\mathbf{r}-\mathbf{r}_0) +\sum_{i=1}^{N} D_i\delta(\mathbf{r}-\mathbf{r}_i). \quad (3)$$

This may be integrated using the Green's function $g_0(\mathbf{r})$ for $\mathcal{H}$ in the absence of scatterers. We set

$$E=\frac{\hbar^2k^2}{2m}. \quad (4)$$

For $E>0$, we impose $k>0$, and

$$g_0(\mathbf{r})=-\frac{m}{2\pi\hbar^2}\frac{e^{ikr}}{r}. \quad (5)$$

For $E<0$, we take $k=iq$, with $q>0$ in Eq. (5). The resulting solution of Eq. (3) in thus

$$G(\mathbf{r},\mathbf{r}_0)=g_0(\mathbf{r}-\mathbf{r}_0)+\sum_{i=1}^{N} D_i g_0(\mathbf{r}-\mathbf{r}_i). \quad (6)$$

The secondary sources amplitudes D_i are then determined by imposing on (6) the contact conditions (1) at the order $O(1)$. That is, for the non-diverging term $1/a_{\rm eff}$

$$\sum_{j=1}^{N} M_{ij}D_j=\frac{2\pi\hbar^2}{m}g_0(\mathbf{r}_i-\mathbf{r}_0),\quad \forall i\in\{1,\ldots,N\} \quad (7)$$

where we have introduced the $N\times N$ matrix

$$M_{ij}=\begin{cases} -\dfrac{2\pi\hbar^2}{m}g_0(\mathbf{r}_i-\mathbf{r}_j) & \text{if } i\neq j,\\ ik+a_{\rm eff}^{-1} & \text{if } i=j.\end{cases} \quad (8)$$

Eq. (7) constitutes the aforementioned $N\times N$ linear system, and its formal solution gives [6]

$$G(\mathbf{r},\mathbf{r}_0)=g_0(\mathbf{r}-\mathbf{r}_0)+\sum_{i,j=1}^{N} g_0(\mathbf{r}-\mathbf{r}_i)[M^{-1}]_{ij}g_0(\mathbf{r}_j-\mathbf{r}_0). \quad (9)$$

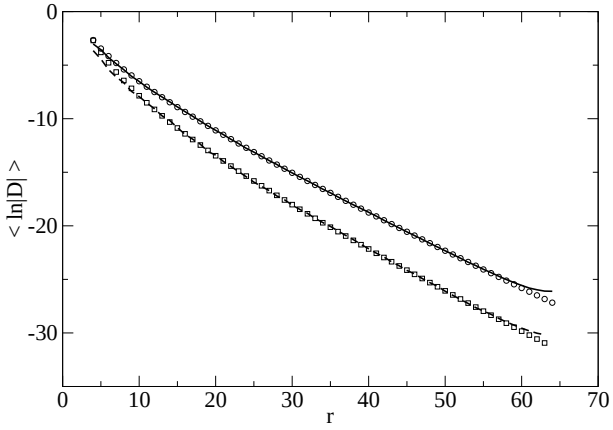

FIG. 3: For the 3D system: Coarse grained histogram $\langle\ln|D|\rangle$ as a function of the distance from the source, for two different kinds of disorder. The first kind of disorder (solid line) is obtained by a random filling of the cubic lattice inside the sphere of radius $R=70d$. A second kind of disorder (dashed line) is obtained first by a random filling of the cubic lattice inside only one sector (1/8) of the sphere, $x>0, y>0, z>0$, and then by filling the remaining seven sectors by reflecting the positions in the first sector with respect to planes $x=0$, $y=0$, $z=0$. The average is taken over 50 realizations of disorder. The filling factor is $p_{\rm occ}=1/10$, the effective scattering length is $a_{\rm eff}=1.0d$ and the energy of the emitting source is $E=\hbar^2k^2/2m$ with $kd=0.1$. The circles represent, for the two kinds of disorder, the fit of the histogram on the interval $10d<r<55d$ to extract the Lyapunov exponent κ with the first method [see Eq. (10)]. We obtain ($\kappa d=0.31$, $\alpha=2.2$), and ($\kappa d=0.31$, $\alpha=3.6$), for the first and second kind of disorder, respectively. The Lyapunov exponents appear to be identical, so that one can use the second kind of disorder to calculate κ with a substantial gain in the computational effort (a factor 64 on the memory size and a factor 512 in the CPU time).

The matrix M will play a crucial role in what follows. Indeed, we will relate the localized eigenmodes of the matter wave to the eigenvectors of the matrix M. This matrix shows a purely off-diagonal disordered coupling between different scatterers, which is long-range at positive energies, and short-range at negative energies. This kind of disorder does not coincide with the one originally introduced by Anderson, characterized by diagonal disorder and short range couplings [1]. Finally, it is worth noticing that this model can be exactly mapped to the case of a scalar light wave scattered by a disordered ensemble of two-level atoms, where the same matrix M appears [22].

III. LOCALIZATION LENGTH

A. Defining and calculating the localization length

In an infinitely extended disordered three-dimensional system, a matter wave of positive energy emitted by a source is expected to be exponentially suppressed (localized) at large distances, if its energy is smaller than a critical energy E_c, the so-called mobility edge. This corresponds to absence of matter wave transport. The localization length ξ is the length scale associated with this exponential decay. It is an average quantity, which has to be calculated by taking the mean over all possible realizations of the disorder. Waves emitted by a source of energy E larger than E_c are instead expected to propagate diffusively in the system, with an intensity decaying as the inverse of the distance.

As we shall see, mobility edges can also be present for negative energies. Indeed, a single matter wave A atom exhibits bound states with a few B scatterers (dimers AB, trimers AB_2, tetramers AB_3, etc.), that have a non-zero hopping amplitude among different scatterers. Then, the evanescent matter wave emitted by a source at negative energy may populate such bound states. This may lead to waves of dimers, trimers, etc., bounded in the volume occupied by the scatterers, but which can be either extended or localized within that volume.

To obtain these properties we thus calculate the Green's function $G(\mathbf{r}, \mathbf{r}_0)$ which gives the $\mathbf{r}$-dependent matter wave amplitude resulting from the source in $\mathbf{r}_0$. In practice we solve numerically the linear system Eq. (7) and we extract the localization length ξ for the amplitudes D_i in two different ways.

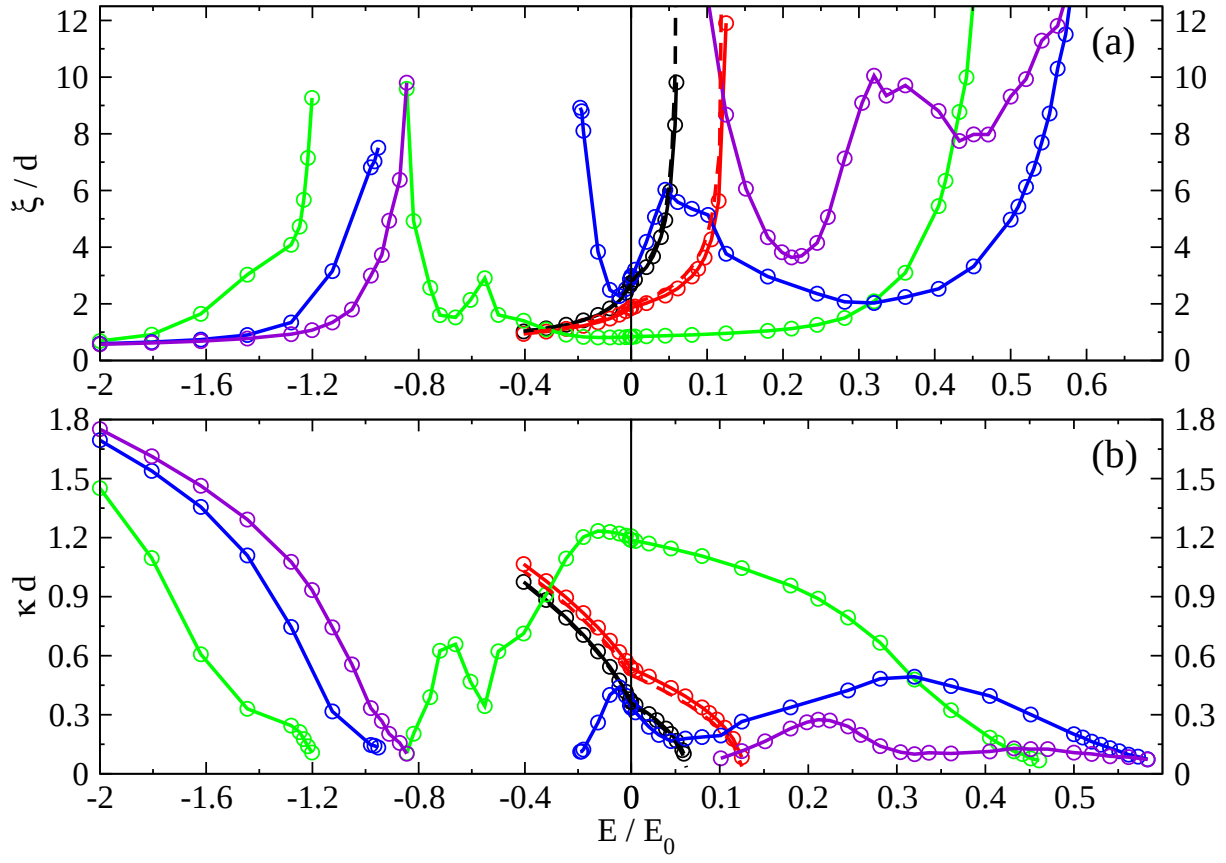

FIG. 4: For the 3D system: Localization length ξ [(a)], and Lyapunov exponents $\kappa = 1/\xi$ [(b)], as a function of the energy E of the emitting source for different values of the effective scattering length $a_{\rm eff}$: $a_{\rm eff} = 0.1d$ (black solid line), $a_{\rm eff} = 0.2d$ (red solid line) , $a_{\rm eff} = 0.7d$ (green solid line), $a_{\rm eff} = 1.0d$ (blue solid line), $a_{\rm eff} = 1.3d$ (violet solid line). The mean field calculation [see Eq. (18)] is also shown for $a_{\rm eff} = 0.1d$ (black dashed line), and for $a_{\rm eff} = 0.2d$ (red dashed line). The lattice spacing d of the cubic lattice, and the energy $E_0 = \hbar^2/(md^2)$, are used as units. Results are obtained using the first method [see Eq. (10)], with 500 realizations of the disorder for $E > 0$ and 100 realizations for $E < 0$. The filling factor is $p_{\rm occ} = 1/10$, and the sphere radius is $R = 70d$, which leads to a mean number of scatterers $\langle N \rangle \approx 1.4 \times 10^5$. Comparing the results for $E > 0$ with 100 and 500 realizations, we estimate that the error on κ is $\approx 10\%$, and even smaller for the lowest values of ξ.

First method: The spatial localization of the Green's function is reflected in a localization of the secondary source amplitudes D_i. We thus calculate the average over disorder $\langle \ln |D_i| \rangle$, and construct a coarse grained histogram of the data set $(|\mathbf{r}_i - \mathbf{r}_0|, \langle \ln |D_i| \rangle)$, that we fit with the functional form

$$|\mathbf{r} - \mathbf{r}_0| \longmapsto \ln \left[C \frac{e^{-\kappa |\mathbf{r} - \mathbf{r}_0|}}{|\mathbf{r} - \mathbf{r}_0|^{\alpha}} \right], \tag{10}$$

where C, α and the Lyapunov exponent κ are the three free parameters. The localization length is then $\xi = 1/\kappa$. The fit is performed over the dipoles with positions $\mathbf{r}_i$ such that $r_{\min} < |\mathbf{r}_i - \mathbf{r}_0| < r_{\max}$, in order to exclude the near-field contribution of the source, and to minimize the effects of the boundaries of the disorder. Both effects are apparent in Fig.1a, which reveals a boundary layer of ≈ 15 lattice spacings. Apart from these boundary effects, the results for increasing radii R of the sphere containing the scatterers are in good agreement, and reveal that the decay of D_i is not simply exponential. On the contrary, the inclusion of the power-law factor in Eq. (10) provides an excellent fit to the numerical data, as shown in Fig.1b. For the system sizes that we are to treat numerically, the failure to include of α as a fitting parameter would lead to unreliable values of κ dependent upon the system size. Finally, we note that the functional form Eq. (10) includes both the localized and the diffusive sides of the phase diagram, with $\xi = +\infty$ in the diffusive regions.

Second method: Inspired by the usual definition of the Lyapunov exponent in one-dimensional disordered systems, we define a direction dependent transmission coefficient $t(\mathbf{n})$ for the field emitted by the source, for a given realization of disorder:

$$G(\mathbf{r}, \mathbf{r}_0) \underset{r \to +\infty}{\sim} t(\mathbf{n}) g_0(\mathbf{r} - \mathbf{r}_0), \tag{11}$$

with the unit vector $\mathbf{n} = \mathbf{r}/r$. Here $f \sim g$ means $f/g \to 1$. This expression, compared with Eq. (6) for $r \to +\infty$, provides the exact relation

$$t(\mathbf{n}) = 1 + \sum_{i=1}^{N} D_i e^{-ik\mathbf{n}\cdot(\mathbf{r}_i - \mathbf{r}_0)}. \tag{12}$$

In the one-dimensional case, the quantity to consider is the logarithm of the transmission coefficient, rather than the coefficient; the former is indeed a self-averaging quantity contrary to the latter [8]. We thus define the direction dependent three-dimensional Lyapunov exponent as

$$\kappa(\mathbf{n}) = -\lim_{R \to +\infty} \frac{\langle \ln |t(\mathbf{n})| \rangle}{R} \quad \text{for } E > 0, \tag{13}$$

$$\kappa(\mathbf{n}) = q - \lim_{R \to +\infty} \frac{\langle \ln |t(\mathbf{n})| \rangle}{R} \quad \text{for } E < 0, \tag{14}$$

where R is the radius of the sphere containing the point-like scatterers and the average is taken over the disorder [9]. The term q in (14) has been introduced since, for $E < 0$, the field emitted by the source $g_0(\mathbf{r} - \mathbf{r}_0)$ taken as a reference field in Eq.(11) decays as e^{-qr} for $r \to \infty$.

We have found numerically that $\kappa(\mathbf{n})$ only weakly depends on the direction so that we may define the localization length in terms of its average over solid angle:

$$\kappa = \frac{1}{\xi} \equiv \int \frac{d^2 n}{4\pi} \kappa(\mathbf{n}). \tag{15}$$

In practice, we calculate the limit in Eq. (13) and (14) by a linear extrapolation to $R^{-1} = 0$ of the values obtained for at least three different values of R^{-1}.

The first and second methods are compared, for a fixed value of the energy E in Fig.2a and for several values of E in Fig.2b, and are found to give compatible values of the Lyapunov exponent. In practice, the first method has the advantage of not requiring a calculation for different values of the radius R, the border effects being eliminated by a suitable choice of the fitting range. Also, the value of $|t(\mathbf{n})|$ is bounded from below by the numerical accuracy ϵ_{num} so that the second method may be used only if $\exp(-\kappa R) \gg \epsilon_{\text{num}}$.

A symmetry trick: In practice, to reduce the computational effort, we have imposed some symmetry properties on the disorder used to obtain the results shown in Figs. 1, 2, 4, 5: We have imposed reflection symmetries with respect to the planes $x = 0$, $y = 0$, $z = 0$ and we have set $\mathbf{r}_0 = \mathbf{0}$, so that the independent unknowns in the linear system Eq. (7) are the amplitudes D_i in the sector $x > 0, y > 0, z > 0$. This effectively reduces the number of unknowns by a factor of 8, resulting in a gain of a factor 64 on the memory size and of a factor 512 in the CPU time, without affecting the value of the Lyapunov exponent κ, as shown in Fig.3.

B. Numerical results for the localization length

Using the first method described in the previous subsection, we have calculated numerically the Lyapunov exponent κ and the localization length $\xi = 1/\kappa$ for different values of the effective scattering length a_{eff}, and of the filling factor p_{occ}, see Figs.4,5,6.

A central point is the choice of the value of p_{occ}. Our scope was to study the regime where the presence of the lattice has a small effect on the localization properties, since we consider here the lattice mainly as an experimental tool to realize strong disorder. To this end we will not investigate the regime where p_{occ} only weakly differs from unit: This regime indeed corresponds to a matter wave propagating in a periodic structure with dilute random vacancies. On the other side, the opposite regime $p_{\text{occ}} \to 0$ is not favorable experimentally since it leads to large localization lengths scaling at least as the mean distance between scatterers $d/p_{\text{occ}}^{1/3}$ [11].

For these reasons, we choose in Fig.4 the reasonable value $p_{\text{occ}} = 0.1$. This figure shows the localization length, see Fig.4a, and the Lyapunov exponent, see

Fig.4b, as a function of the energy E of the emitting source, both for negative and positive values of E. Several values of $a_{\rm eff}$ are considered in this figure.

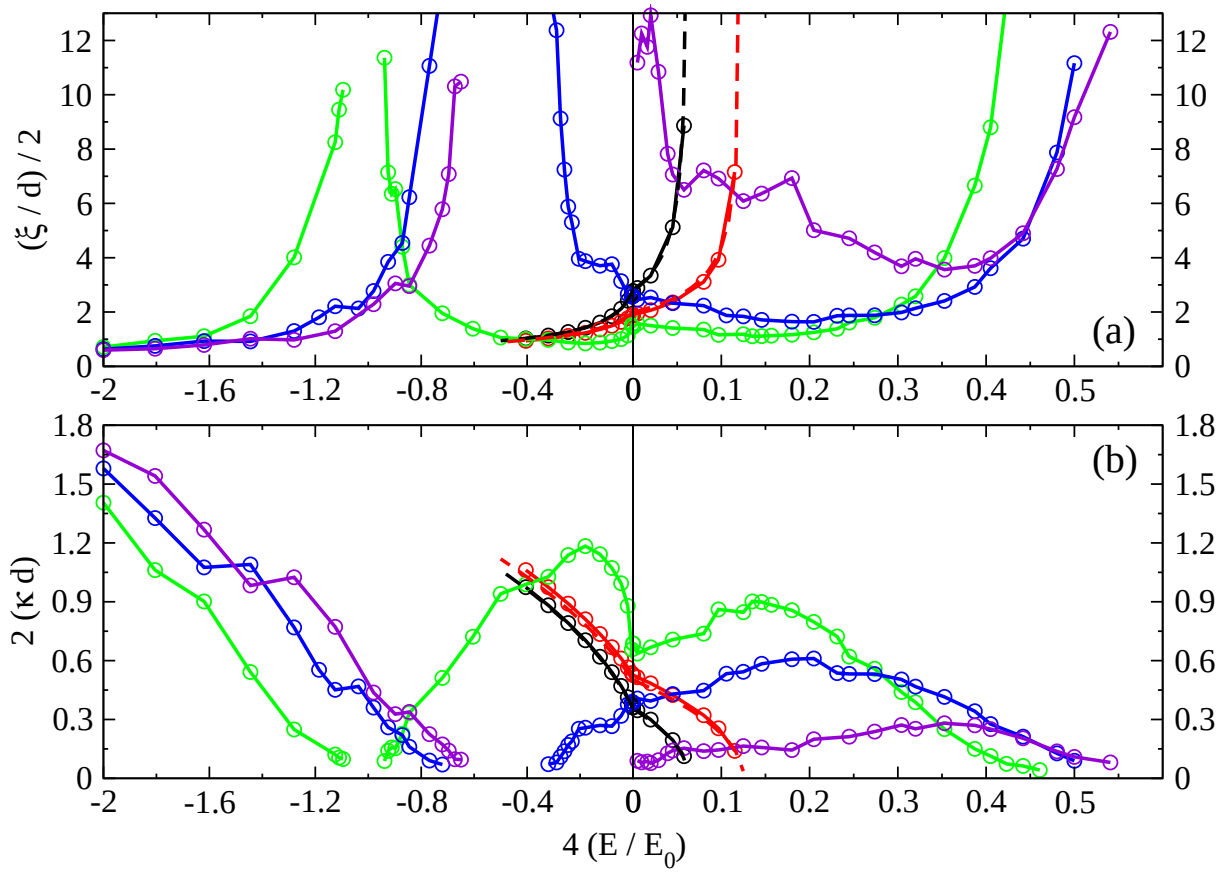

FIG. 5: The same as Fig. 4, except that: The value of $p_{\rm occ}$ is 1/80, the radius is $R = 140d$ (corresponding to a mean number of scatterers $\langle N\rangle \approx 1.4\times 10^5$), and $a_{\rm eff}$ is rescaled to have the same values of $\rho^{1/3}a_{\rm eff}$ as in Fig. 4, where $\rho = p_{\rm occ}/d^3$ is the mean density of scatterers. Since $p_{\rm occ}^{1/3}$ is two times smaller as compared to Fig. 4, we have $a_{\rm eff} = 2\times 0.1d$ (black solid line), $a_{\rm eff} = 2\times 0.2d$ (red solid line) , $a_{\rm eff} = 2\times 0.7d$ (green solid line), $a_{\rm eff} = 2\times 1.0d$ (blue solid line), $a_{\rm eff} = 2\times 1.3d$ (violet solid line). The axes are rescaled accordingly, to allow a direct comparison with the results of Fig. 4. The number of realizations of disorder is equal to 100 for all points.

The values $a_{\rm eff}/d \ll 1$ are easy to analyze in a perturbative picture: The matter wave inside the cloud of scatterers experiences a mean field shift equal to $\rho g_{\rm eff}$ where $\rho = p_{\rm occ}/d^3$ is the mean density of scatterers and $g_{\rm eff} = 4\pi\hbar^2 a_{\rm eff}/(2m)$ is the effective coupling constant between the matter wave and a scatterer. In this mean field model, the Green's function is simply that of a free matter wave in the presence of the uniform mean field shift $\rho g_{\rm eff}$ inside the sphere. We then have, for $r < R$ and $r_0 < R$

$$\langle \mathbf{r}|\frac{1}{E+i0^+-\mathcal{H}_{\rm mf}}|\mathbf{r}_0\rangle \simeq -\frac{m}{2\pi\hbar^2}\frac{e^{ik_{\rm mf}r}}{r}, \qquad (16)$$

with $\mathcal{H}_{\rm mf} = H + \rho g_{\rm eff}$. The wave vector is then given by

$$E = \frac{\hbar^2 k^2}{2m} = \frac{\hbar^2 k_{\rm mf}^2}{2m} + \rho g_{\rm eff}. \qquad (17)$$

The mean field prediction is thus that, for $E < \rho g_{\rm eff}$, $k_{\rm mf}$ is purely imaginary, the matter wave cannot propagate in the gas of scatterers and is damped with a Lyapunov exponent

$$\kappa_{\rm mf}^2 = 4\pi\rho a_{\rm eff} - k^2. \qquad (18)$$

The two conditions of validity for the this mean field prediction are that (i) the matter wave scattering on a single scatterer should be in the regime of the Born approximation, $|ka_{\rm eff}| \ll 1$, and (ii) there should be a large

mean number of scatterers within the volume $\xi_{\rm mf}^3$, that is $\rho\xi_{\rm mf}^3 \gg 1$, so one may neglect fluctuations in the density of scatterers over the scale $\xi_{\rm mf}$. The mean field prediction (18) is plotted as a dashed line in Fig. 4 over the range $E < \rho g_{\rm eff}$, for the two lowest values of $a_{\rm eff}/d$, where it is in good agreement with the numerical results. For $E > \rho g_{\rm eff}$, the mean field picture can of course not predict how the Green's function decays with $|\mathbf{r}-\mathbf{r}_0|$. In the numerical approach, the localization length turns out to be too large to be determined in a reliable way for the accessible system sizes.

In the regime $E > \rho g_{\rm eff}$, we have found a second manifestation of the mean field potential $\rho g_{\rm eff}$. In an optical analogy, this potential creates a discontinuity in the refractive index for the matter wave at the border of the sphere containing the scatterers, the index passing from unity outside the sphere to $n \approx (1 - \rho g_{\rm eff}/E)^{1/2}$ within. This induces a reflection of the matter wave, with a Fresnel reflection coefficient $r = (n-1)/(n+1)$. Since the source position $\mathbf{r}_0$ is in the center of the sphere, this gives rise to a radial stationary matter wave with an intensity contrast $(I_{\rm max} - I_{\rm min})/(I_{\rm max} + I_{\rm min}) = 2|r|/(1+|r|^2)$, provided that one can neglect the attenuation of the coherent part of the matter field, that is if the mean free path $\approx 1/(\rho\sigma_{\rm scatt})$, with $\sigma_{\rm scatt} = 4\pi a_{\rm eff}^2$, is larger than the sphere radius. We have indeed observed this phenomenon numerically.

For larger values of $a_{\rm eff}$, of the order of the lattice spacing d, Fig. 4 shows an interesting structure of maxima and minima of the Lyapunov exponent at both positive and negative energies.

For $E > 0$, the value of $a_{\rm eff} = 0.7d$ shows a wide region of remarkably small values of the localization length, with $\xi \approx d$ even smaller than the mean distance between scatterers. For larger values of E, a sharp rise of ξ is observed. A natural question is whether this rise may be attributed to the presence of a mobility edge. This requires a proof of the presence of localized states to the left of this "edge". This will be addressed in section IV, where the presence of localized states will be confirmed for $a_{\rm eff}/d = 1$ and 1.3, in contrast to the cases $a_{\rm eff}/d = 0.1, 0.2$ and 0.7. A careful study of the corresponding phase transition and its critical exponents requires an examination of finite size scaling that we leave for future work.

Another interesting point is that, further increasing the value of $a_{\rm eff}/d$, although intuitively it must be tough to increase the strength of disorder, actually leads to larger values of ξ/d. In particular, at unitarity ($a_{\rm eff}/d \to +\infty$) our system sizes were too small to allow a reliable determination of ξ. Similarly, for negative values of $a_{\rm eff}/d$, we have not obtained evidence of a finite ξ. This is consistent with the prediction, based on a perturbative calculation of the transport mean free path, that no matter wave localization can take place for $a_{\rm eff} < 0$ [12].

For $E < 0$, it there appears in Fig. 4 an energy interval where the localization length takes very large values. At first sight, this may be surprising, as one may naively expect e.g. from Eq. (18), that κ is an increasing function of $|E|$ at least equal to $(2m|E|)^{1/2}/\hbar$. In the case where $a_{\rm eff}$ is much smaller than the mean distance between scatterers, we relate the existence of this energy interval to the fact that the matter wave can form a bound state (a dimer) of wavefunction $\phi_0(\mathbf{r}-\mathbf{r}_i)$ with each scatterer i, of spatial extension $a_{\rm eff}$ and of energy [10]

$$E_{\rm dim} = -\frac{\hbar^2}{2ma_{\rm eff}^2}. \tag{19}$$

The various probability amplitudes to have the dimer on the sites $\mathbf{r}_i$, $\mathbf{r}_j$, ..., are then coupled by transition amplitudes $t_{\rm trans}$ of the order of $E_{\rm dim}$ times overlap integrals between $\phi_0(\mathbf{r}-\mathbf{r}_i)$ and $\phi_0(\mathbf{r}-\mathbf{r}_j)$, integrals that drop exponentially with the distance as $\exp(-|\mathbf{r}_i - \mathbf{r}_j|/a_{\rm eff})$. A precise calculation gives a transition amplitude between two scatterers separated by a distance r_{ij} [30]

$$t_{\rm trans}(r_{ij}) = -\frac{\hbar^2}{ma_{\rm eff}}\frac{e^{-r_{ij}/a_{\rm eff}}}{r_{ij}}. \tag{20}$$

Over the energy interval roughly extending around $E_{\rm dim}$ with a width of the order of typical values of $|t_{\rm trans}|$, we then face the problem of a bound state that can "tunnel" from one scatterer to another, which may result in a localization length ξ. It turns out that this length may have sharp rises as a function of energy, suggesting the occurrence of two mobility edges. This picture cannot of course be quantitative for values of $a_{\rm eff}$ as large as $0.7d$, but it correctly predicts that the negative energy interval of large values of ξ shifts to higher energies and broadens, when one increases $a_{\rm eff}/d$.

In Fig. 5 we consider the same problem as in Fig. 4 with a much smaller filling factor $p_{\rm occ} = 1/80$. We considered values of $a_{\rm eff}$ such that $\rho^{1/3}a_{\rm eff}$ is the same for the two figures. We also rescaled the axes of the figure so that two identical values of the abscissa for Fig. 4 and Fig. 5 correspond to an identical value of $mE/(\rho^{2/3}\hbar^2)$, and two identical values of the ordinate correspond to an identical value of $\rho^{1/3}\xi$. This allows us to see the effect of the underlying lattice [11]. There are some quantitative (not qualitative) differences between the two figures. In particular, at negative energies, the separation between the energies where ξ has a sharp rise is smaller in the case of $p_{\rm occ} = 1/80$ than in the case of $p_{\rm occ} = 1/10$ and the periodic case $p_{\rm occ} = 1$ (as we will see in Fig. 6), on the rescaled energy axis.

Finally, we consider in Fig. 6 the "periodic" case corresponding to $p_{\rm occ} = 1$. In this case, a non-zero value of κ is not an effect of disorder but rather results from the existence of forbidden energy bands. For $E < 0$ we recover the same physics due to the existence of a dimer, leading here to the emergence of an allowed energy band for the dimer. For $E > 0$, the dependence of ξ with the energy is more flat than in the disordered case, except close to the band edges where it diverges. We note that the forbidden band is quite broad for values of $a_{\rm eff}$ of the order of the lattice spacing or larger.

IV. DENSITY OF LOCALIZED STATES

Calculation of the localization length, as defined in the previous section, is not sufficient to prove the existence of localized states at the considered energy. E.g. it is expected that, in a spectral gap of the system, the localization length is finite whereas there is no state available. In the present section, we directly investigate the presence of localized states as a function of the energy E.

A. Method

We have to distinguish two cases, according to the sign of the energy E.

Negative energies: For $E < 0$, the eigenstates of the matter wave are discrete bound states. Such a bound state corresponds to the matter wave being trapped by the gas of scatterers, but it is not necessarily a localized state. In particular, in the limit $0 < a_{\rm eff}$ smaller than the mean distance between scatterers, we recall the picture of a $A - B$ dimer that may tunnel from one scattering site to another, see subsection III B, and this dimer, with a negative total energy, may be delocalized over the whole gas of scatterers.

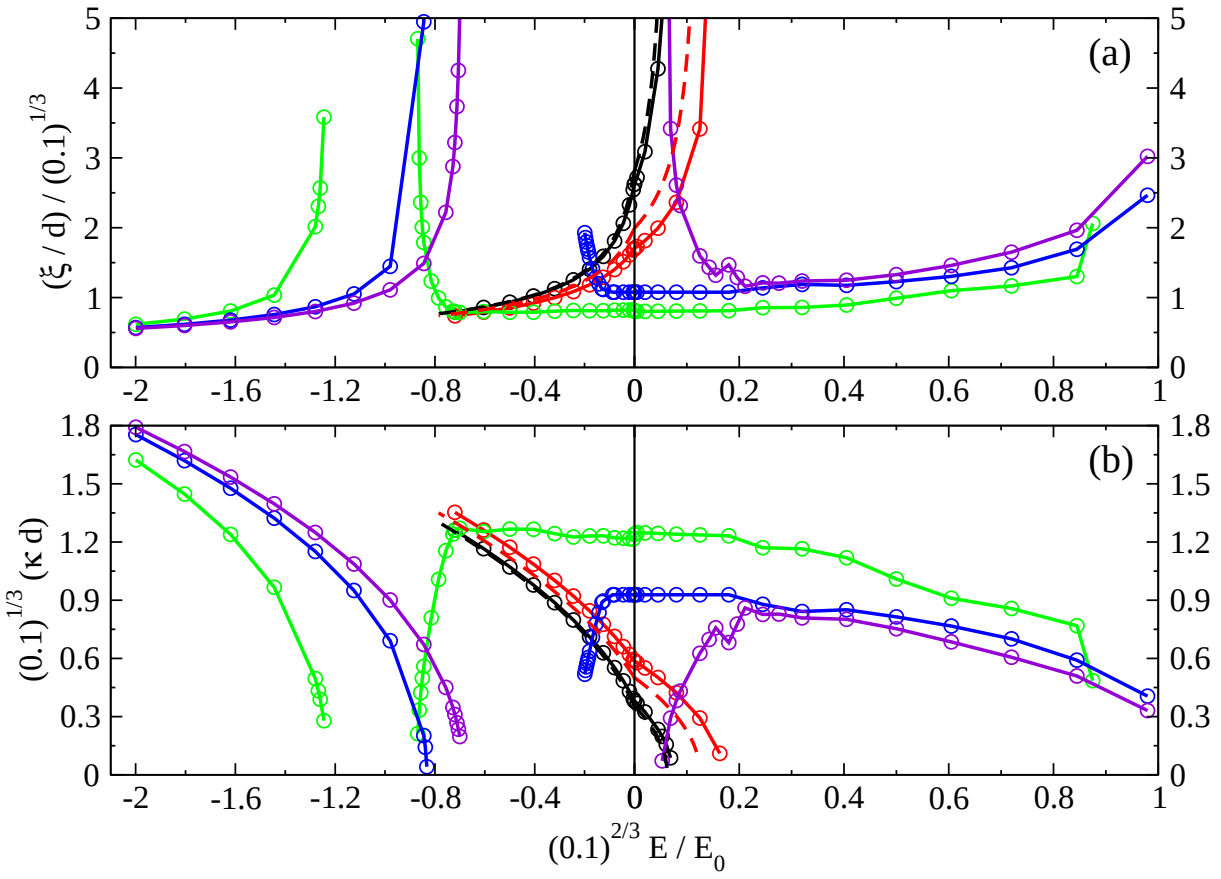

FIG. 6: The same as Fig. 4, except that: The value of $p_{\rm occ}$ is 1 (there is no disorder, since all the lattice sites within the sphere of radius $R = 30d$ are occupied by the scatterers, which leads to $N \approx 1.1 \times 10^5$ [13]), and $a_{\rm eff}$ is rescaled to have the same values of $\rho^{1/3} a_{\rm eff}$ as in Fig. 4, where $\rho = p_{\rm occ}/d^3$ is the mean density of scatterers. Since $p_{\rm occ}^{1/3}$ is $(0.1)^{1/3}$ times smaller as compared to Fig. 4, we have $a_{\rm eff} = (0.1)^{1/3} \times 0.1d$ (black solid line), $a_{\rm eff} = (0.1)^{1/3} \times 0.2d$ (red solid line) , $a_{\rm eff} = (0.1)^{1/3} \times 0.7d$ (green solid line), $a_{\rm eff} = (0.1)^{1/3} \times 1.0d$ (blue solid line), $a_{\rm eff} = (0.1)^{1/3} \times 1.3d$ (violet solid line). The axes are rescaled accordingly, to allow a direct comparison with the results of Fig. 4.

The bound state eigenenergies correspond to poles of the Green's function Eq.(2). Since $G(\mathbf{r}; \mathbf{r}_0)$ diverges for

such an eigenenergy, the secondary source amplitudes D_i diverge in Eq.(6), or equivalently, according to Eq.(7), this implies that the matrix M defined in Eq.(8) has a zero eigenvalue. For $E < 0$, the matrix M is real and symmetric, so has N real eigenvalues m_i. To find the bound state energies, there are two strategies.

In the first strategy, one works for a fixed value of the effective scattering length $a_{\rm eff}$, one numerically calculates the N eigenvalues $m_i(E, a_{\rm eff})$, $1 \leq i \leq N$, and then solves for E each implicit equation

$$m_i(E, a_{\rm eff}) = 0. \tag{21}$$

This may be done efficiently by dichotomy, using the property that m_i is a monotonically increasing function of E (see appendix A). In the second strategy, one inverts the problem, working for a fixed value of the energy E and solving $m_i(E, a_{\rm eff}) = 0$ for $a_{\rm eff}$. This turns out to be straightforward, because of the following structure of the matrix M [6]:

$$M = \frac{1}{a_{\rm eff}}{\rm Id} + M_\infty(E) \tag{22}$$

where M_∞ depends only on the energy, not on the effective scattering length. For each value of E, one then simply has to diagonalize $M_\infty(E)$, with resulting eigenvalues $m_i^\infty(E)$. From the relation $m_i(E, a_{\rm eff}) = a_{\rm eff}^{-1} + m_i^\infty(E) = 0$, one obtains the following parameterization of the negative eigenenergy branches:

$$\frac{1}{a_{\rm eff}} = -m_i^\infty(E). \tag{23}$$

Positive energies: Let us consider first the ideal case of scatterers extending over the entire position space. Then, for $E > 0$ two kinds of states are expected, square integrable localized states corresponding to a discrete spectrum, and extended states corresponding to a continuous spectrum. It is expected that the continuous spectrum exists at $E > E_{\rm c}$, where E_c is called a mobility edge, and that the localized states are essentially at $E < E_c$ [16].

In reality, the scatterers occupy a finite volume of radius R, so that, for $E > 0$, the energy spectrum of the matter wave forms a continuum extending from 0 to $+\infty$, and none of the positive energy eigenstates is square integrable. Nevertheless, for a large enough radius R, one can still find eigenstates which, inside the medium, exponentially decrease over several orders of magnitude away from a central region, toward the borders of the gas of scatterers [6]. For all practical purposes, these are localized states. From a spectral point of view, these localized states are expected to correspond to very narrow resonances of the matter wave inside the scattering medium, that is to *complex* poles

$$z_{\rm res} = E_{\rm res} - i\hbar\Gamma/2 \tag{24}$$

of the Green's function Eq.(2) analytically continued to the lower half of the complex plane, $\Gamma > 0$. Such a resonance, localized close to the center, has a width Γ, i.e. an inverse lifetime, that vanishes exponentially with the radius R as $\exp(-2R/\xi)$, where ξ is the localization length of the localized states [6, 12], reproducing for $R = +\infty$ the aforementioned ideal case of poles on the real axis.

To find such resonances, one has to analytically extend the Green's function Eq.(2) to complex energies z. Then, setting $k = (2mz/\hbar^2)^{1/2}$ in Eq.(5), taking the real and negative axis as the line cut for $z^{1/2}$, one finds that Eq.(9) still holds. Then the complex poles $z_{\rm res}$ are such that the matrix M has a zero eigenvalue. Adopting the second strategy used for bound states, one actually diagonalizes $M^\infty(z)$ so that has to solve the equations for $z_{\rm res}$:

$$\frac{1}{a_{\rm eff}} = -m_i^\infty(z_{\rm res}). \tag{25}$$

In practice, to solve Eq.(25), we implement Newton's method as follows. We choose some real and positive value for E. We diagonalize $M^\infty(E)$, calculating the eigenvalues and the eigenvectors; we select an eigenvalue $m_i^\infty(E)$ and we set the effective scattering length to the value such that $a_{\rm eff}^{-1} + m_i^\infty(E)$ is purely imaginary,

$$a_{\rm eff} = -\frac{1}{{\rm Re}\, m_i^\infty(E)}. \tag{26}$$

This constitutes the initial guess in Newton's method. The successive steps of the method involves the calculation of the derivative of $m_i^\infty(z)$ with respect to z, which can be done thanks to the extension of the Hellmann-Feynman theorem to non-hermitian matrices [20]. Of particular interest is the approximate value of $z_{\rm res}$ obtained after the first step:

$$z_{\rm res} = E - i\frac{{\rm Im}\, m_i^\infty(E)}{dm_i^\infty(E)/dE}, \tag{27}$$

which, if compared with (24), provides the values of $E_{\rm res}$ and Γ. We have checked that, if the imaginary part of $m_i^\infty(E)$ is small enough, typically $\lesssim 10^{-3}/d$ for $p_{\rm occ} = 0.1$, the first step Eq.(27) has in practice already converged to the exact pole location. To obtain Fig.7, we used this first step approximation.

B. Results for the density of bound states and resonances

Using the techniques presented in the previous subsection, we have calculated the density of resonances and of bound states in the plane $(E, a_{\rm eff})$, E being the real part of Green's function complex poles for resonances and the eigenenergy for bound states. The raw result is presented in Fig.7a.

For large and negative E, and *positive* $a_{\rm eff}$, a first class of bound states is observed, with a density of states concentrated in a narrow interval of values of $a_{\rm eff}$. This was expected: For $a_{\rm eff} > 0$ the matter wave can form a bound state (a dimer) with a single scatterer, of energy $E_{\rm dim}$ given by Eq.(19). In the presence of the disordered ensemble of scatterers, this dimer subsists in the limit $a_{\rm eff} \ll \rho^{-1/3}$, where ρ is the mean density of scatterers. Simply, the dimer state may tunnel from one scatterer in location $\mathbf{r}_i$ to another one in $\mathbf{r}_j$, with a tunneling amplitude close to Eq.(20). This tunneling broadens the eigenenergy interval around $E_{\rm dim}$ by an amount of the order of the tunneling amplitude, a small amount in relative value if $a_{\rm eff} \ll \rho^{-1/3}$.

As one moves to larger values of the energy, the aforementioned interval of eigenenergies moves toward larger values of $a_{\rm eff}$ and broadens, as expected from the previous reasoning. In addition, an internal structure is apparent in the figure, see the zoom in Fig.8, the density of states being peaked over several subintervals, corresponding to various branches. These branches may be identified physically by calculating the eigenenergies of trimers, tetramers, ... of the matter wave with two, three, ... scatterers on the lattice, see the lines in the corresponding Fig.8. One simply has to apply the method described in the previous subsection, for $N = 2, 3, \ldots$, see Eq.(23), and the corresponding matrices $M(E)$ may be diagonalized analytically. Setting $E = -\hbar^2 q^2/(2m), q > 0$, one finds that $a_{\rm eff}$ is given as a function of the energy of a AB_2 trimer by the two branches

$$\frac{1}{a_{\rm eff}} = q \pm \frac{e^{-qr_{12}}}{r_{12}} \tag{28}$$

where r_{12} is the distance between the two B scatterers. The calculation may be done also for the AB_3 tetramers, giving rise to three branches for each particular set of values of the inter-scatterer distances r_{12}, r_{13}, r_{23}. The analytical expressions are simple in the relevant case $r_{13} = r_{23}$, where one sets $\beta = e^{-qr_{12}}/r_{12}$ and $\delta \equiv e^{-qr_{13}}/r_{13}$. One then finds that one of the branches reduces to one of the trimer branches, $1/a_{\rm eff} = q + \beta$. The other two branches are then given by [10]:

$$\frac{1}{a_{\rm eff}} = q - \frac{1}{2}\left[\beta \pm (\beta^2 + 8\delta^2)^{1/2}\right]. \tag{29}$$

For negative values of E close to the origin, another class of bound states is observed for *negative* $a_{\rm eff}$. For values of $a_{\rm eff}$ close to zero, this class may be interpreted by a simple mean field effect. The matter wave experiences an effective attraction inside the volume containing the scatterers, represented by the negative mean field potential $\rho g_{\rm eff}$, see Eq.(17), so that the gas of scatterers produces an effective square well potential of radius R that can support matter wave bound states. This mean field interpretation is in good agreement with the numerical results for small $|a_{\rm eff}|$. The oblique mean field white line in Fig.7 giving the bottom $\rho g_{\rm eff}$ of the effective square well potential accurately reproduces the lower boundary of the bound state energies.

Each of the two components that we discussed for $E < 0$ continuously develops in two corresponding components on the $E > 0$ side of Fig.7a.

The component in the lower part of Fig.7a has a first boundary (delimiting a blue triangular zone containing no resonances) which is well described by mean field theory at low values of E and $a_{\rm eff}$, see the oblique white line. It has a second boundary on the right, corresponding to a blue oval region again with no resonances. There is no physical interpretation of this blue oval region at the present moment. A word of caution may be useful at this stage. For $E > 0$, we calculate a density of resonances, with an approximate method valid for long-lived resonances only (see subsection IV A), so the absence of resonances does not imply the absence of eigenstates (in particular *extended* states) of the system. The blue oval region thus does not necessarily corresponds to a spectral gap in the density of states. In particular, the calculation of the localization length ξ performed in the previous section for $a_{\rm eff}/d = 0.1$ shows a divergence of ξ at the mean field border, with small values of ξ at energies below this border, which is compatible with a spectral gap. However it does not show any sharp decrease of ξ at the border with the oval region, ξ retains very high values even for energies in the oval region, raising doubts about the existence of a spectral gap in that region. As we shall see in Fig.7b, the component in the lower part of Fig.7a contains no long lived resonances, hence no localized states.

The $E > 0$ component in the upper part of Fig.7a is more promising for observing localized states. In Fig.7b we have kept only very long-lived resonances, with a decay rate $\Gamma < 10^{-6}\hbar/(md^2)$ [21]. This corresponds to a lifetime larger than $\simeq$ 200s for ^{87}Rb atoms in an optical lattice of spacing $d = 0.4\mu$m [14]. We see that, after this selection, the upper component still gives a significant contribution, while the lower component essentially disappears.

In Fig.7c and Fig.7d, we have kept only the bound states and resonances that are localized in real space, according to the two following criteria respectively: In Fig.7c we keep states with a participation volume $V_{\rm p}$ smaller than $(6.5d)^3$, where the participation volume is defined as:

$$V_{\rm p} \equiv \frac{1}{\rho \sum_{i=1}^{N} |D_i|^4} \tag{30}$$

where the amplitudes D_i are the components of the eigenstates of the M matrix with a zero eigenvalue, and are normalized such that $\sum_{i=1}^{N} |D_i|^2 = 1$. In Fig.7d we keep states with a root-mean square size σ in real space smaller than $4.2d$, with the definition

$$\sigma^2 \equiv \left(\sum_{i=1}^{N} r_i^2 |D_i|^2\right) - \left(\sum_{i=1}^{N} \mathbf{r}_i |D_i|^2\right)^2, \tag{31}$$

where the D_i are defined as for $V_{\rm p}$.

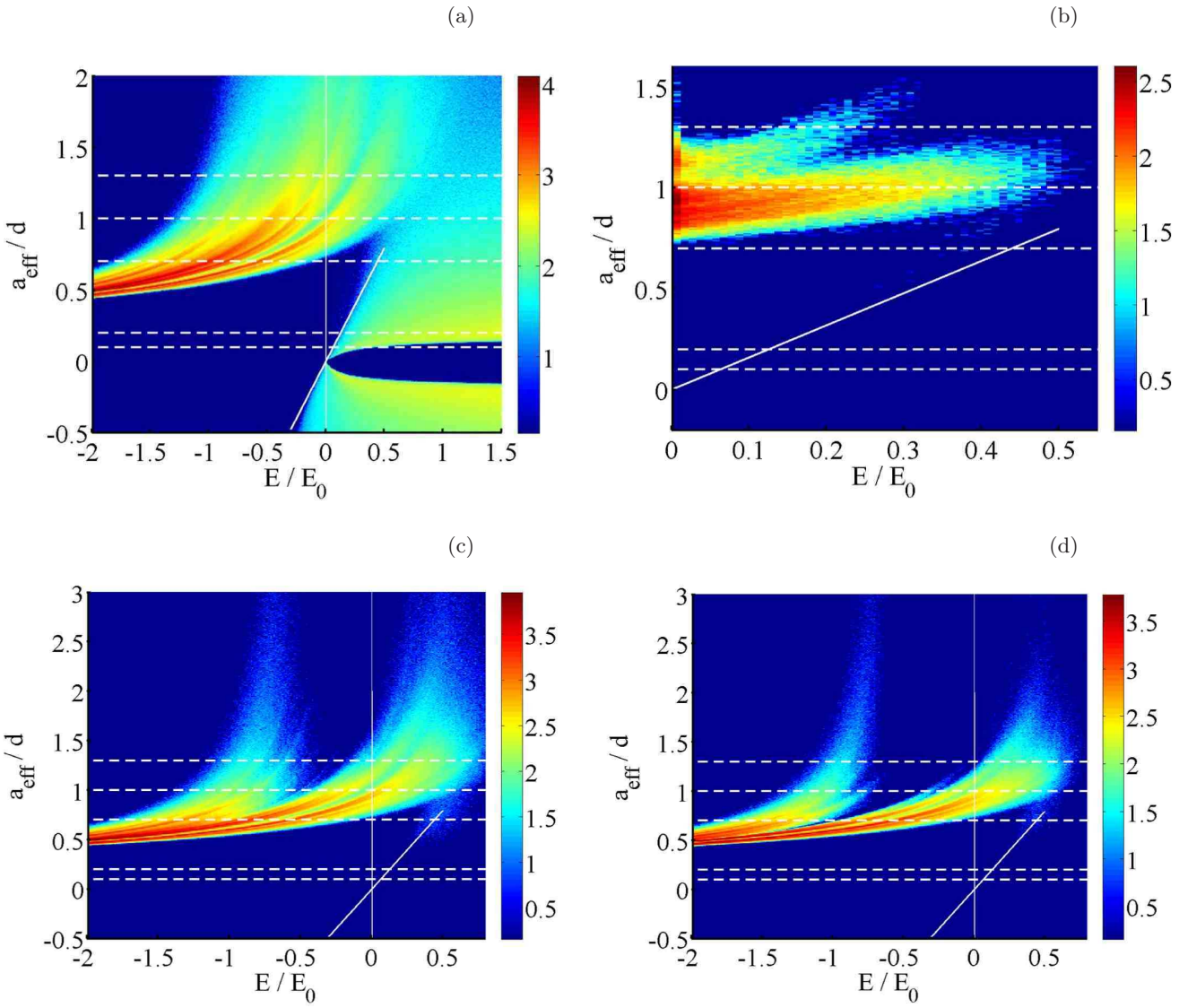

FIG. 7: For the 3D system: Density of resonances and bound states per scatterer in the plane (energy E, effective scattering length $a_{\rm eff}$), obtained as explained in subsection IV A. E on the horizontal axis is either the real part of $z_{\rm res}$ on the positive energy side, or the bound state eigenenergy on the negative energy side. The filling factor is $p_{\rm occ} = 1/10$ within a sphere of radius $R = 29d$, so that the mean number of scatterers is $\langle N\rangle \approx 10^4$. The value of E is discretized with a step $0.0025E_0$ for both positive and negative values of E, and we use $E_0 = \hbar^2/(md^2)$ as unit of energy. For each value of E one different realization of disorder is used, without imposing any reflection symmetry (see end of subsection III A). A logarithmic scale is used: The color map (see bar on the right) is applied to the quantities $\log_{10}\frac{N_{\rm res}}{N}\frac{E_0 d}{\delta S}$, for $E > 0$, and $\log_{10}\frac{N_{\rm bound}}{N}\frac{E_0 d}{\delta S}$, for $E < 0$, where $N_{\rm res}$ and $N_{\rm bound}$ are the number of resonances and bound states respectively, within each rectangular bin of area $\delta S = \delta E \delta a_{\rm eff}$ ($\delta E = 0.01E_0$ and $\delta a_{\rm eff} = 0.007d$, for both positive and negative values of E). The plotted quantity is then $\simeq \log_{10}(1.4N_{\rm res})$, and $\simeq \log_{10}(1.4N_{\rm bound})$, respectively. The horizontal dashed lines correspond to the values of $a_{\rm eff}/d \in \{0.1, 0.2, 0.7, 1, 1.3\}$ used in Fig. 4. The oblique solid line is the border of the energy gap $E = \rho g_{\rm eff}$ predicted by the mean field theory (see Eq.(18) with $\kappa_{\rm mf} = 0$). (a) No selection is applied to the resonances ($E > 0$). As explained in the text, most of the displayed resonances (the ones with too large a width) are not expected to be meaningful. (b) Restricting to $E > 0$, only the resonances with a width $\Gamma < \Gamma_{\rm max} = 10^{-6}E_0/\hbar$ are kept in the density of resonances. The value of $\Gamma_{\rm max}$ is essentially infinite with respect to the duration of typical experiments: For a matter wave of ^{87}Rb atoms and an optical lattice with $d = 0.4\mu$m, as in [14], one has indeed $1/\Gamma_{\rm max} \simeq 200$ seconds. (c) Only the resonances and bound states corresponding to a small enough participation volume V_p are kept in the density ($V_p^{1/3}/d < 6.5$, see Fig.9a and c). (d) Only the resonances and bound states corresponding to a small enough r.m.s. size σ in real space are kept in the density ($\sigma/d < 4.2$, see Fig.9b and d).

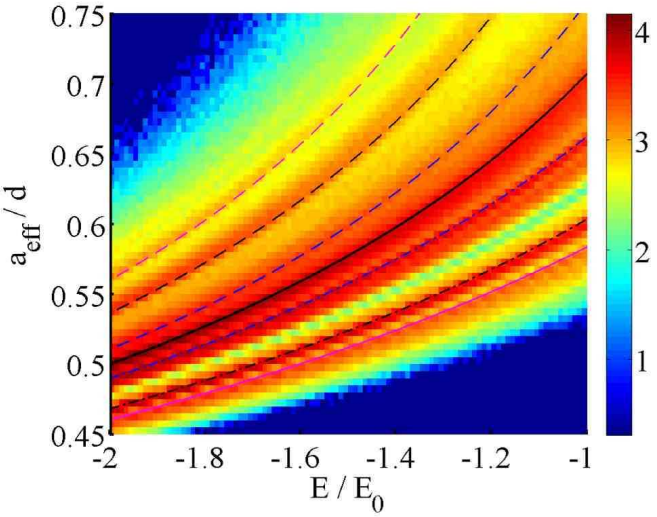

FIG. 8: Zoom of figure 7a, in the region of $E < 0$ and small and positive values of $a_{\rm eff}$ (here $\delta E = 0.01E_0$, and $\delta a_{\rm eff} = 0.005d$). On the color map representing the density of states (see caption of Fig.7a), are plotted the energies of bound states of an A atom with one, two or three B atoms, denoted respectively dimer AB, trimer AB_2, and tetramer AB_3 states. In particular are plotted the energies of a dimer Eq.(19) (black solid line), of a trimer Eq.(28) with two B atoms separated by a distance $r_{12} = d$ (dashed black and dash-dotted black lines), of a trimer with two B atoms separated by a distance $r_{12} = \sqrt{2}d$ (dashed and dash-dotted blue lines), and of a tetramer Eq.(29) with three B atoms separated by distances $r_{13} = r_{23} = d$ and $r_{12} = \sqrt{2}d$ (solid and dashed magenta lines). It is worth noting that the prediction for the energy of such isolated bound states correspond to the higher density lines of the color map plot.

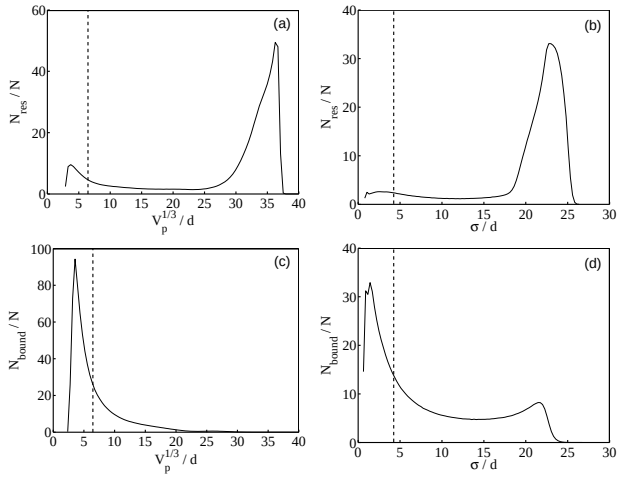

FIG. 9: For the 3D system: For all resonances with $E_{\rm res}/E_0 \in (0, 2)$ and and $a_{\rm eff}/d \in (-3, 3)$, and all bound states with $E \in (-2, 0)E_0$ and $a_{\rm eff}/d \in (-3, 3)$, the figures show an histogram giving the number of resonances (in (a) and (b)) and bound states (in (c) and (d)) per scatterer (the number of scatterers is $N = 10^4$) as a function of: in (a) and (c), the square root of the participation volume defined in Eq.(30); in (b) and (d), the r.m.s. size in real space defined in Eq.(31). The bin size is $\sim 0.2d$ for (a) and (c), and $\sim 0.26d$ for (b) and (d). The parameters are the same as in Fig. 7a. The dashed vertical lines are the values $V_{\rm p}^{1/3}/d \simeq 6.5$ and $\sigma/d \simeq 4.2$ [15] used in Fig. 7c and Fig. 7d to select the bound states and resonances that are spatially localized and to filter out the bound states and resonances that are spatially extended.

For computational convenience, in defining these two quantities we used the amplitudes D_i, rather than the wavefunctions ψ of the resonances and the bound states. We verified for several examples that localization of D_i implies a localization of ψ, and vice versa. This can be easily understood since the matter wave problem is analogous to that of a scalar wave of light scattered by pinned atomic dipoles. In this case, the values of D_i correspond to the values of the electric dipole moment on each atom, and the matter wave wavefunction ψ corresponds to the electric field $\mathcal{E}$. In this scalar light analogy it is intuitive that the spatial extension of the dipoles reflect that of the electric field, and vice versa [22]. For completeness, we provide the expression of ψ in terms of D_i in the appendix B.

The choice of above mentioned limiting values for $V_{\rm p}$ and σ are motivated by the histograms of Fig.9. For $E > 0$, the histograms clearly reveal a bimodal structure in the probability distribution of $V_{\rm p}$ and σ, which suggests the coexistence of localized resonances (small values of $V_{\rm p}^{1/3}$ and σ) and extended resonances (large values of $V_{\rm p}^{1/3}$ and σ, of the order of the radius $R = 29d$ of the sphere containing the scatterers). For $E < 0$, the bimodal structure is still apparent for σ, showing that some bound states are extended. Interestingly, the bimodal structure is not present for $E < 0$ on the histogram of $V_{\rm p}^{1/3}$. Actually, it may happen that a state which is a coherent superposition of a few-body bound state (e.g. a dimer, a trimer) at different locations is considered as a localized state with the criterion based on $V_{\rm p}$, whereas it is considered as an extended state with the one based on σ. An extreme example of such a case corresponds to a dimer delocalized over two sites of positions $\mathbf{r}$ and $-\mathbf{r}$. Then $D_i = (\delta_{\mathbf{r}_i,\mathbf{r}} + \delta_{\mathbf{r}_i,-\mathbf{r}})/\sqrt{2}$, leading to $V_{\rm p}^{1/3} = (2/\rho)^{1/3}$ (insensitive to the distance $2r$ between the two possible dimer locations), and to $\sigma = r$ [31].

Coming back to Fig.7d, we thus see two main streams of localized states, one restricted to negative energies, and the other extending to positive energies. The existence of these two streams explains the structure of the localization length in Fig.4a. It is possible to establish a correspondence between the occurrence of divergences of the localization length, and boundaries between an energy interval with localized states and an energy interval with extended states. A particularly rich example corresponds to the effective scattering length value $a_{\rm eff} = d$, for which by combining the information coming from the localization length ξ in Fig.4a, and the density of reso-

nances/bound states in Figs.7a and 7d, we can distinguish 5 energy intervals:

- $E/E_0 < -1.3$: the density of bound states is zero in Fig.7a, and ξ takes small values Fig.4a. This reflects the occurrence of an energy gap.
- $-1.3 < E/E_0 < -1$: the density of localized bound states is non-zero in Fig.7d, and ξ increases with a divergent behavior at $E/E_0 \simeq -1$ in Fig.4a. This suggests the presence of an energy band of localized states with an upper mobility edge at $E/E_0 \simeq -1$.
- $-1 < E/E_0 < -0.2$: there are bound states in Fig.7a, but no localized bound states in Fig.7d, and ξ assumes very large values (presumably larger than the system size). This suggests the presence of an energy band of extended bound states delimited by two mobility edges at $E/E_0 \simeq -1$ and $E/E_0 \simeq -0.2$.
- $-0.2 < E/E_0 < 0.6$: the density of localized bound states and localized resonances is non-zero in Fig.7d, and ξ assume small values away from divergent behaviors at $E/E_0 \simeq -0.2$ and $E/E_0 \simeq 0.6$ in Fig.4a. This suggests the presence of an energy band of localized states delimited by two mobility edges at $E/E_0 \simeq -0.2$ and $E/E_0 \simeq 0.6$.
- $E/E_0 > 0.6$: the density of localized resonances is zero in Fig.7d, and ξ assumes very large values (presumably larger than the system size). This suggests the presence of an energy band of extended states delimited by a lower mobility edges at $E/E_0 \simeq 0.6$.

One can apply the same analysis to other values of $a_{\rm eff}$ considered in Fig.4a. In particular, it is interesting to note that for $a_{\rm eff} = 0.7d$ the correspondence between the positions of mobility edges deduced from the localization length ξ, and deduced from the density of resonances/bound states, is only qualitative: for negative energies, ξ diverges at $E/E_0 \simeq -1.2$ and $E/E_0 \simeq -0.8$ in Fig.4a, while one finds the transition region between localized and extended states at $E/E_0 \simeq -1.0$ and $E/E_0 \simeq -0.9$ in Fig.7d. This discrepancy can be explained in terms of finite size effects, as is apparent from Fig.10. Indeed, Fig.10a shows a zoom of the figure 7d (i.e. density of resonances and bound states per scatterer in the plane (E,$a_{\rm eff}$) having a r.m.s. size in real space $\sigma < 4.2d$). In Fig.10b we impose an additional filtering with respect to that of Fig.10a: we keep only bound states and resonances having their maximum $|D_i|$ at a distance less than $R' = 20d$ from the origin, whereas the disorder fills a sphere of radius $R = 30d$. In this way only localized states located far from the border of the system are selected. In figure 10b the transition region between localized and extended states is now at $E/E_0 \simeq -1.2$ and $E/E_0 \simeq -0.8$, in quantitative agreement with the mobility edges deduced from ξ in Fig.4a.

To conclude the analysis of the 3D system, we give in Fig.11 the values of the width Γ for the resonances in the plane $(E, a_{\rm eff})$. A filtering was applied to these resonances: In Fig.11a we considered only resonances with a participation volume $V_{\rm p}^{1/3}/d \leq 6.5$, and in Fig.11b only resonances with a r.m.s size in real space $\sigma/d \leq 4.2$. This analysis shows the presence of numerous extremely long-lived resonances with $\Gamma \leq 10^{-6} E_0/\hbar$. This figure may be useful for experimental purposes to identify optimal values of $(E, a_{\rm eff})$ for the observation of maximally localized

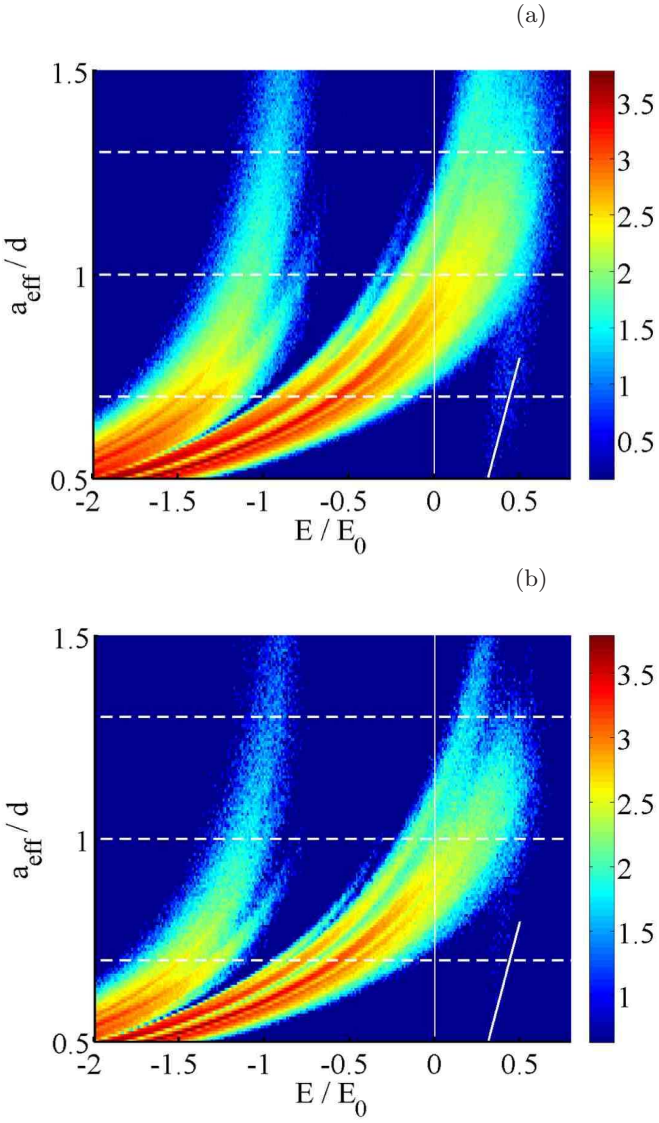

FIG. 10: For the 3D system: Finite size effect on the density of localized states. (a) Zoom of the figure 7d, which shows the density of resonances and bound states per scatterer in the plane (E,$a_{\rm eff}$) having a r.m.s. size in real space $\sigma < 4.2d$. We recall that there are $N \simeq 10^4$ scatterers in a sphere of radius $R = 29d$. (b) Same as (a), with an additional filtering: we keep only bound states and resonances having their maximum $|D_i|$ at a distance less than $R' = 20d$ from the origin (in the normalization, we considered the number of atoms $N' \simeq 3.3 \times 10^3$ in the sphere of radius R').

resonances. These occur for values of $a_{\rm eff} \approx 0.8d$ and $0 < E/E_0 < 0.4$, for the considered density of scatterers $p_{\rm occ} = 1/10$.

V. LOCALIZATION IN A 2D GEOMETRY

It is now experimentally possible to realize systems where the atomic matter wave atom A is confined in a 2D geometry. One can apply a strong confinement along the direction z, freezing the motion in its ground state along z, while leaving a free motion in the xy plane. In analogy with the 3D disordered system studied in previous sections, we study here the 2D case, where both B scatterers and matter wave atoms A are confined along the z direction (not necessarily with the same potential), and B scatterers are randomly distributed at the nodes of a $2D$ optical lattice in the xy plane (the A atoms being insensitive to that lattice). As for the 3D case, the low energy scattering of an A atom with a single trapped B atom can be characterized by a $2D$ effective scattering length, accounting for the effect of the atomic motion of the B atom during the scattering process. This allows us to replace the B atoms by point-like scatterers at fixed positions, described by contact conditions on the A atom wavefunction. For simplicity we use for the effective scattering length in 2D the same notation $a_{\rm eff}$ as in 3D. To our knowledge, the dependence of the effective 2D scattering length on the free space 3D scattering length a, on the atomic masses and on the oscillation frequencies, has not yet been investigated.

On the theoretical side there has been significant investigation of disordered systems in 2D since this is the lower critical dimension for the occurrence of the metal-insulator transition. In 2D it is expected that all states are localized in an infinite system, but the localization length increases rapidly with the energy [17, 23]. It is thus important to identify the range of parameters (matter wave energy E and $a_{\rm eff}$) for which the localization length ξ takes small values. In subsection V A we explain how to adapt the 3D formalism to the 2D case, and in subsection V B we present the results for the localization length and the density of localized states.

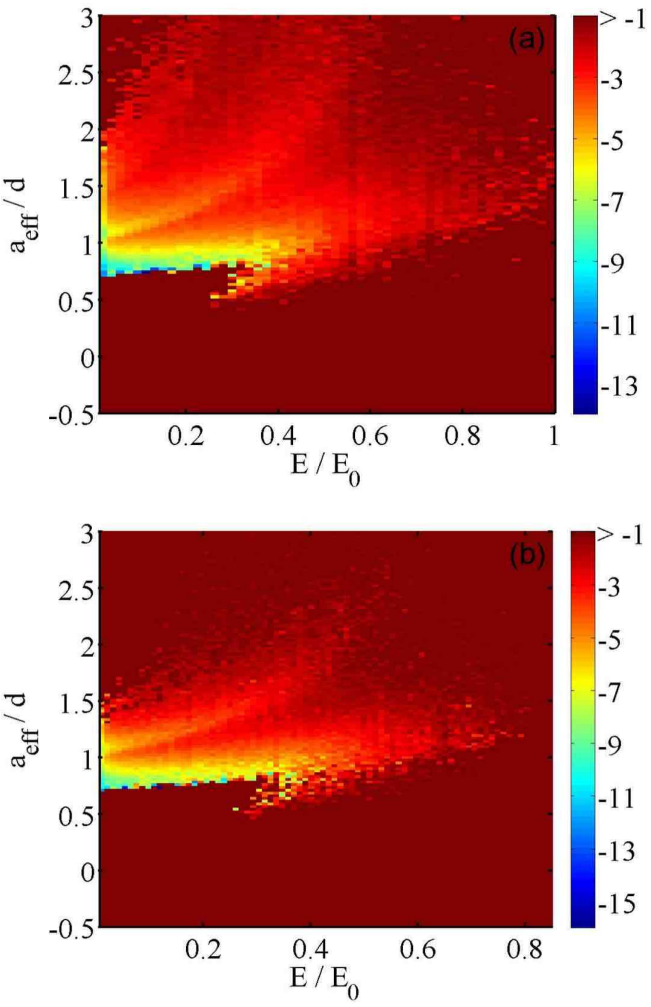

FIG. 11: For the 3D system: Width Γ of the resonances as a function of the energy E and the effective scattering length $a_{\rm eff}$ [see Eqs. (24) and (27)]. The physical parameters are the same as in Fig. 7. The plane $(E, a_{\rm eff})$ is decomposed in rectangular bins of widths δE and $\delta a_{\rm eff}$. The color map (see bar on the right) is applied to the quantity $\log_{10} \hbar\langle\Gamma\rangle/E_0$ where $\langle\Gamma\rangle$ is the mean value of Γ for the resonances within a given bin. The resonances are filtered in (a) over the participation volume as in Fig. 7c and in (b) over the r.m.s. size σ as in Fig. 7d. In (a) one has $\delta E = 0.009E_0$ and $\delta a_{\rm eff} = 0.02d$, and in (b) one has $\delta E = 0.008E_0$ and $\delta a_{\rm eff} = 0.02d$.

A. Formalism for 2D systems

In 2D the contact condition on the matter wave wavefunction in the vicinity of each scatterer of position $\mathbf{r}_i$ is

$$\psi(\mathbf{r}) = \frac{m}{\pi\hbar^2} D_i \ln(|\mathbf{r} - \mathbf{r}_i|/a_{\rm eff}) + O(|\mathbf{r} - \mathbf{r}_i|) \qquad (32)$$

where $a_{\rm eff}$ is now the 2D effective scattering length (always positive) [24]. Comparing to the 3D contact conditions Eq.(1), we see that $-1/\ln(a_{\rm eff}/d)$ in 2D plays the role of $a_{\rm eff}/d$ in 3D. We recall that, in 2D, the limit $a_{\rm eff} \to 0$ does in fact correspond to a weakly repulsive limit, while $a_{\rm eff} \to +\infty$ corresponds to a weakly attractive limit.

The 2D Green's function still obeys Eq.(3), so that formally Eq.(6) still holds provided that one takes for g_0 the 2D free matter wave Green's function. For $E > 0$, we set $E = \hbar^2k^2/(2m)$, $k > 0$, and we obtain

$$g_0(\mathbf{r}) = -\frac{im}{2\hbar^2} H_0^{(1)}(kr) \qquad (33)$$

with the Hankel function expressed in terms of Bessel functions as $H_0(z) = J_0(z) + iN_0(z)$. From [25] one ob-

tains the limiting behaviors

$$H_0^{(1)}(kr) \underset{r\to+\infty}{\sim} \left(\frac{2}{\pi kr}\right)^{1/2} e^{i(kr-\pi/4)}, \quad (34)$$

$$H_0^{(1)}(kr) \underset{r\to 0}{\sim} 1+\frac{2i}{\pi}\ln\left(\frac{kre^{\gamma}}{2}\right)+o(1), \quad (35)$$

where $\gamma = 0.57721566\ldots$ is Euler's constant. The numerical factor in Eq.(33) thus results from the fact that $\Delta_{\mathbf{r}} \ln r = 2\pi\delta(\mathbf{r})$ in 2D. For $E < 0$, we set $E = -\hbar^2 q^2/(2m)$, $q > 0$. That is, $k = iq$ is now purely imaginary, and we obtain

$$g_0(\mathbf{r}) = -\frac{m}{\pi\hbar^2} K_0(qr) \quad (36)$$

where K_0 is a modified Bessel function of the second kind.

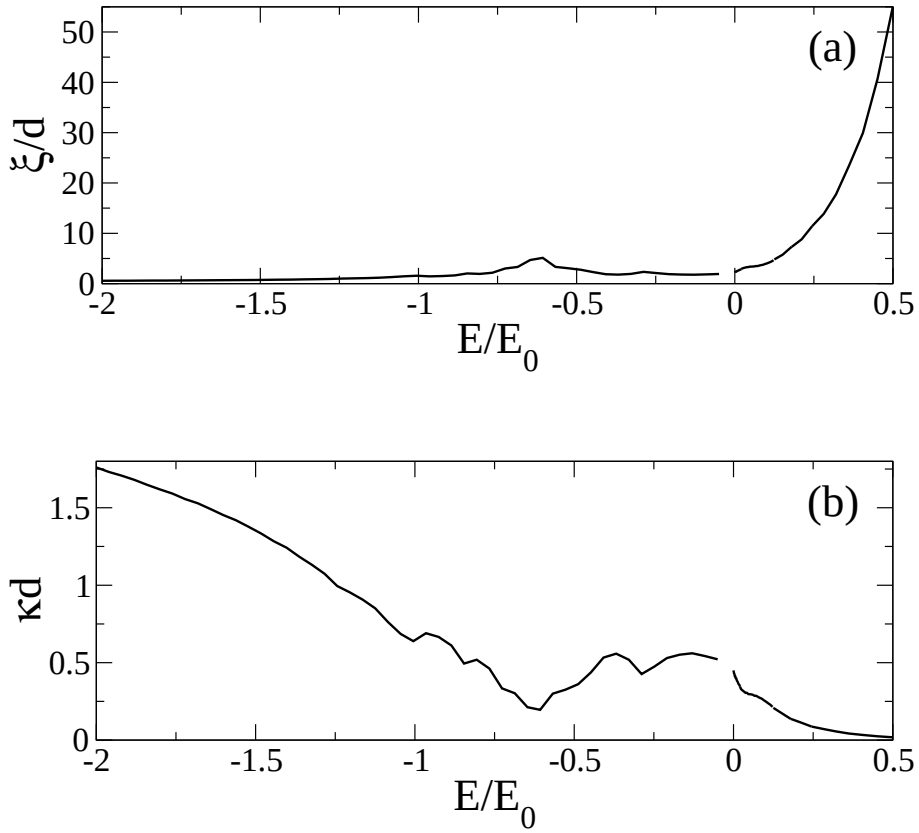

FIG. 12: For the 2D system: localization length ξ (a), and Lyapunov exponent κ (b), as a function of the energy E. Here the 2D effective scattering length is $a_{\rm eff} = d$, the lattice filling factor is $p_{\rm occ} = 1/10$, and an average over 100 realizations for the positions of the scatterers has been performed. The value of κ is obtained using the second method [see Eqs.(39) and (40)]. For values of $0 < E/E_0 < 0.24$, we considered larger and larger system sizes $2R/d \in \{100, 150, 250, 350\}$ until a convergent value for κ is reached, within the statistical error bars, which are smaller than 5%. For $0.24 < E/E_0 < 0.5$ we considered system sizes $2R/d \in \{350, 600\}$, and found a maximal deviation of 10% in κ between the two sizes, finally plotting the values for $2R/d = 600$. For negative energies $-2 < E/E_0 < 0$ we considered system sizes $2R/d \in \{100, 250\}$, from which we extrapolated linearly to the case $1/R \to 0$. In this region we obtain error bars smaller than 1%.

The secondary source amplitudes D_i are then determined by imposing the contact conditions (32) at the order $O(1)$. That is, for the non-diverging term $\ln a_{\rm eff}$,

$$\sum_{j=1}^{N} M_{ij} D_j = -\frac{\pi\hbar^2}{m} g_0(\mathbf{r}_i - \mathbf{r}_0), \quad \forall i \in \{1, \ldots, N\} \quad (37)$$

where we have introduced the $N \times N$ matrix

$$M_{ij} = \begin{cases} \dfrac{\pi\hbar^2}{m} g_0(\mathbf{r}_i - \mathbf{r}_j) & \text{if } i \neq j, \\ -i\frac{\pi}{2} + \ln\left(\frac{k a_{\rm eff} e^{\gamma}}{2}\right) & \text{if } i = j. \end{cases} \quad (38)$$

For $E < 0$, where $k = iq$, $q > 0$, this holds with the determination $\ln i = i\pi/2$, leading to the diagonal element $M_{ii} = \ln\left(\frac{q a_{\rm eff} e^{\gamma}}{2}\right)$.

For the calculation of the localization length ξ, we use the second method already discussed for the 3D case. By following the same derivation as in 3D, and using Eq.(34), we obtain the same expression (12) for the values of the transmission amplitude $t(\mathbf{n})$ of a source located at the position $\mathbf{r}_0$. Then, we define the Lyapunov exponent κ as

$$\kappa = -\lim_{R\to+\infty} \int_0^{2\pi} \frac{d\theta}{2\pi} \frac{\langle \ln|t(\mathbf{n})|\rangle}{R} \text{ for } E > 0, \quad (39)$$

$$\kappa = q - \lim_{R\to+\infty} \int_0^{2\pi} \frac{d\theta}{2\pi} \frac{\langle \ln|t(\mathbf{n})|\rangle}{R} \text{ for } E < 0, \quad (40)$$

where $\mathbf{n}$ has coordinates $(\cos\theta, \sin\theta)$ in the xy plane, and R is the radius of the disk containing the disorder.

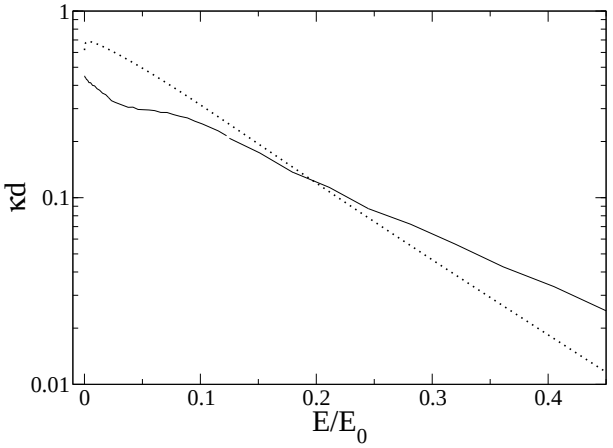

FIG. 13: For the 2D system: Lyapunov exponent κ of Fig.12b, plotted in logarithmic scale (solid black line). The prediction of the independent scattering approximation (ISA) theory is also shown (dotted black line).

To obtain the density of bound states and resonances in 2D, we use the same procedure as in 3D, and split the matrix M as

$$M = \ln(a_{\rm eff}/d)\mathrm{Id} + M_\infty, \quad (41)$$

where M_∞ is the value of M for $1/\ln(a_{\rm eff}/d) = \infty$, i.e. comes from setting $a_{\rm eff} = d$ in Eq.(38). To evaluate the density of bound states for a fixed value of $a_{\rm eff}$ one can solve by dichotomy the 2D equivalent of Eq.(21), using the fact that the eigenvalues of $M(E)$, for $E < 0$, are a monotonically decreasing function of E (see appendix A).

B. Results for the localization length and the density of states for the 2D system

In figures 12a and b we show the value of the localization length ξ and of the Lyapunov exponent $\kappa \equiv 1/\xi$ of Eqs.(39) and (40), as a function of the energy E of the matter wave, for the 2D effective scattering length $a_{\rm eff} = d$. We note a monotonically increasing behavior of ξ, and a monotonically decreasing behavior of κ with the energy E, with the occurrence of a flatter region (a "shoulder") around $E/E_0 = 0.05$. The logarithmic plot for κ in Fig.13 suggests an exponential decay of κ at large energies. However, being over less than one decade, it is not fully conclusive. We also performed calculations of κ for $a_{\rm eff}/d = 0.3$, obtaining similarly large values of κ at low energy. In contrast, for $a_{\rm eff}/d = 3$ the values of κ drop by an order of magnitude for the same energy interval. In Fig.13 we also plot the prediction coming from the frequently used independent scattering approximation (ISA) (see, for instance [26]), according to which the localization length $\xi = l\exp(\pi l \mathrm{Re}k_{\rm eff}/2)$, is expressed in terms of the mean free path $l \equiv 1/(2\mathrm{Im}k_{\rm eff})$, and an effective wavevector $k_{\rm eff}$ defined as

$$E \equiv \frac{\hbar^2 k^2}{2m} = \frac{\hbar^2 k_{\rm eff}^2}{2m} + \rho\langle \mathbf{k}|T(E + i0^+)|\mathbf{k}\rangle \quad (42)$$

where T is the T-matrix in 2D for a single scatterer [27]:

$$\langle \mathbf{k}|T(E + i0^+)|\mathbf{k}\rangle = \frac{-\pi\hbar^2/m}{\ln(k a_{\rm eff} e^{\gamma}/2) - i\pi/2}. \quad (43)$$

The figure shows that the ISA is not accurate for the considered parameters, i.e. for large values of $a_{\rm eff}$, of the order of the mean distance between scatterers.

In figure 14 we show the density of bound states and resonances in the $(E/E_0, \ln(a_{\rm eff}/d))$ plane, in a 2D system (see sections IV A and V A). Calculations have been performed for a disk of radius $R = 150d$, and a density of scatterers $p_{\rm occ} = 1/10$. In Fig.14a we show raw data without any selection, in Fig.14b we present only resonances with a width $\Gamma < 10^{-6}E_0/\hbar$, in Fig.14c we present only resonances and bound states with a participation surface $S_p^{1/2}/d < 9.5$ (this value is motivated by Figs.17a and c, see below), and in Fig.14d we present only resonances and bound states with r.m.s. size $\sigma/d < 4.2$ (this value is motivated by Figs.17b and d, see below). Here

$$S_{\rm p} \equiv \frac{1}{\rho\sum_{i=1}^N |D_i|^4} \quad (44)$$

where the D_i are normalized as $\sum_{i=1}^N |D_i|^2 = 1$, and σ is defined by the 2D version of Eq.(31).

In figure 15 we show a zoom of Fig.14a in the region of lowest energies. The streams of higher densities of bound states are shown to be in correspondence with the energy of some few body bound states (AB dimers, AB_2 trimers, AB_3 tetramers). We recall that, in 2D, the matter wave has a single bound state AB on a isolated scatterer, with an energy [10, 24]

$$E_{\rm dim} = -\frac{2\hbar^2}{m a_{\rm eff}^2\, e^(2\gamma)}. \qquad (45)$$

The energy $E_{\rm trim} = -\hbar^2 q^2/(2m)$ of the AB_2 trimer is given by [10]

$$\frac{a_{\rm eff}\, e^{\gamma}}{2} = \frac{1}{q}\exp\left[\pm K_0(q r_{12})\right], \qquad (46)$$

where r_{12} is the distance between the two B scatterers. The energy $E_{\rm tetra} = -\hbar^2 q^2/(2m)$ of the AB_3 tetramer is given [10], in the particular case of $r_{13} = r_{23}$, by the expression

$$\frac{a_{\rm eff}\, e^{\gamma}}{2} = \frac{1}{q}\exp\left\{\frac{1}{2}[\beta \pm (\beta^2+\delta^2)^{1/2}]\right\}, \qquad (47)$$

where $\beta = K_0(q r_{12})$, $\delta = K_0(q r_{13}) = K_0(q r_{23})$, and r_{ij} is the distance between the two B scatterers i and j. The signature left by few body bound states in the density of states can be further appreciated in Fig.16, where we plot the density of states as a function of the energy $E < 0$, at the fixed value of $a_{\rm eff} = d$. The energies of some few body bound states (vertical arrows in the figure) are shown to correspond to peaks in the density of states. The same calculation, performed for $a_{\rm eff} = 3d$, shows a broad structure where essentially all the peaks are washed out.

In figure 17 we show histograms of the number of states as a function of the participation surface $S_{\rm p}$ and of the r.m.s. size σ, for positive energies (Figs.17a and b) and for negative energies (Figs.17c and d). The structure of the histograms at positive energies shows broad structures corresponding to states extending over the whole disordered system. This fact does not contradict the general statement that all states are localized in a 2D system [23]. Indeed, at large energies and large values of $a_{\rm eff}$, the localization length ξ becomes very large, larger than the system size. For negative energies, the histograms show one narrow peak with no tails, indicating that all the states are localized with a localization length of few lattice spacing only.

In figures 18a and b, we plot the value of the width Γ of the resonances, on the $(E/E_0, \ln(a_{\rm eff}/d))$ plane. In Fig.18a, we considered only resonances with a participation surface $S_{\rm p}^{1/2}/d < 9.5$, while in Fig.18b, we considered only resonances with a r.m.s size $\sigma/d < 4.2$. In both figures wide regions are present corresponding to very small values of Γ, i.e. to extremely long-lived resonances (in practice infinitely long-lived at the scale of the experiments).

VI. CONCLUSION

We performed a quantitative study of the 3D and 2D strong localization of matter wave in a random potential realized by point-like scatterers (atoms) pinned at the nodes of a cubic or square lattice. This model allows an exact numerical analysis of both the localization length and density of states, as a function of the matter wave energy and of the effective scattering length between the matter wave and a single scatterer. We considered systems having a number of scatterers of the same order as that achieved in current experiments with ultra cold atomic gases ($N \sim 10^5$), corresponding to systems with a diameter ~ 140 lattice spacings in 3D for a lattice filling factor $= 1/10$.

In 3D, we found evidences for the occurrence of several energy mobility edges, for both positive and negative matter wave energies E. For $E > 0$, we found a mobility edge for a positive effective scattering length of the order of the mean distance between scatterers. For a too large positive, or for a negative value of $a_{\rm eff}$ we found no evidence of mobility edge, in agreement with the predictions in [12]. For $a_{\rm eff}$ small and positive we found the occurrence of an energy gap between $E = 0$ and an upper bound coinciding with a mean field effect $E = g_{\rm eff}\rho$ where ρ if the density of scatterers, and $g_{\rm eff} = 2\pi\hbar^2 a_{\rm eff}/m$. Within this energy gap, there is a small localization length with no evidence of localized states [32]. For $E < 0$, where the matter wave is bound inside the gas of scatterers (a case not explored in previous works to our knowledge), we found localized bound states and evidence of two mobility edges separated by an energy interval where only extended bound states are present. We also found, for $a_{\rm eff}$ small and negative, extended bound states in the energy interval between the mean field shift $E = \rho g_{\rm eff}$ and $E = 0$. To ascertain the presence of the mobility edges, and to identify the universality class of this disorder induced transition, a dedicated analysis should be undertaken using finite size scaling techniques to determine the critical exponent. For experimental purposes, large values of the effective scattering length may be obtained by using Feshbach resonances to control the free space scattering length a [6]. Recently $a > 1\mu$m has been obtained with Li gases [28].

In 2D, no evidence of mobility edges is found for either positive or negative energies. Contrary to the 3D case, at negative energies, all bound states are localized. We identified regions in the $(E/E_0, ln(a_{\rm eff}/d))$ plane where the localization length is small and the density of states is high. This happens for $a_{\rm eff}$ of the order of the average distance between scatterers, for a wide interval of energies. At high energies we find a rapid, exponential-like increase of the localization length with energy. At negative energies the localization length shows no such rapid increase of ξ. To our knowledge, large values of the 2D effective scattering length have not yet been observed. It is thus interesting to study the dependence of the 2D $a_{\rm eff}$ with respect to the free space scattering length a, and

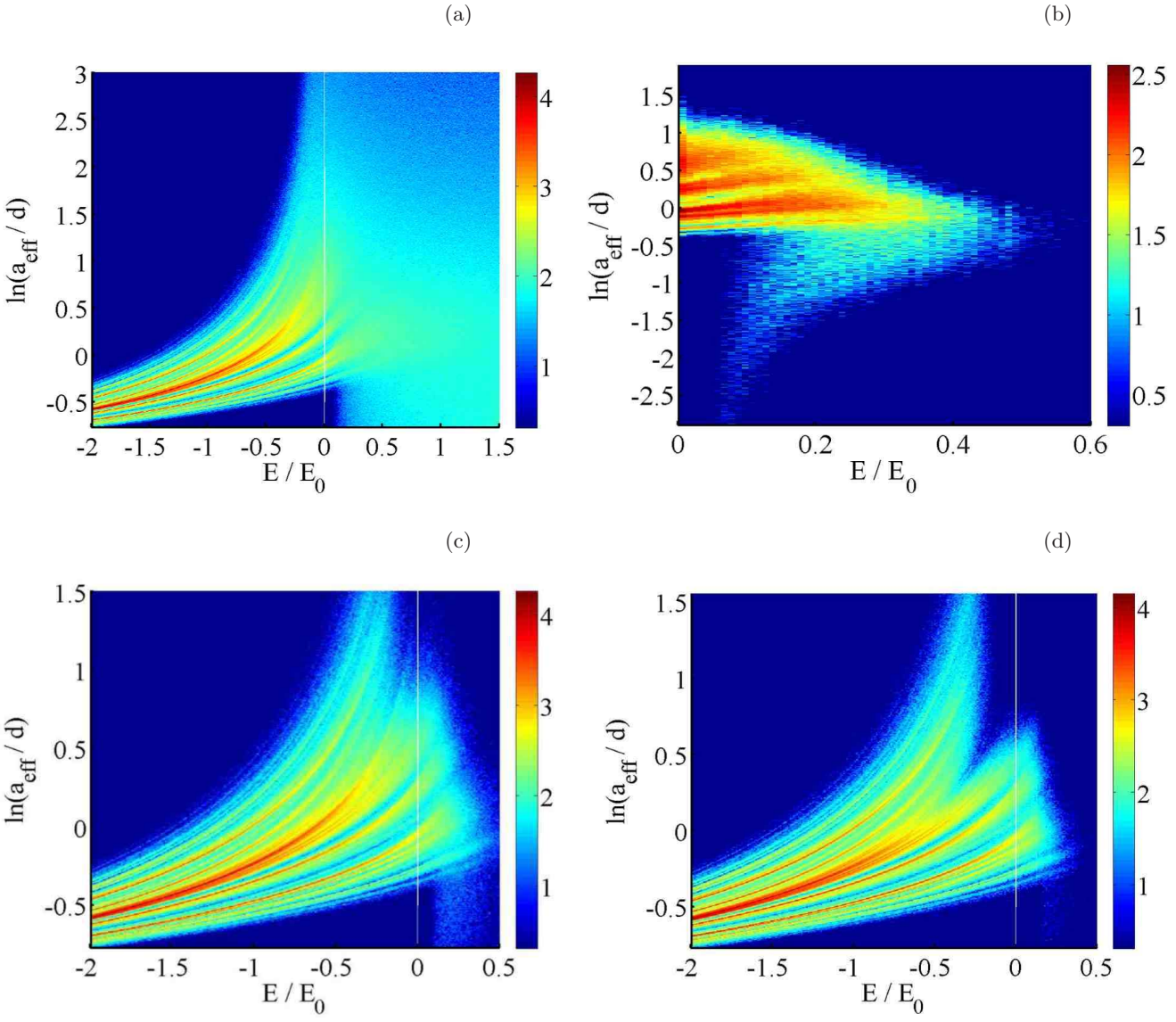

FIG. 14: For the 2D system: Density of resonances and bound states per scatterer in the plane (energy E/E_0, logarithm of the effective scattering length $\ln(a_{\rm eff}/d)$), obtained as explained in the subsection V A. E on the horizontal axis is either the real part of $z_{\rm res}$ on the positive energy side, or the bound state eigenenergy on the negative energy side. The filling factor is $p_{\rm occ} = 1/10$ within a disk of radius $R = 150d$, so that the mean number of scatterers is $\langle N\rangle \approx 7\times 10^3$. The value of E is discretized with a step $0.0025E_0$ for both positive and negative values of E, and we used $E_0 = \hbar^2/(md^2)$ as unit of energy. For each value of E one different realization of disorder is used, without imposing any reflection symmetry (see end of subsection III A). A logarithmic scale is used: The color map (see bar on the right) is applied to the quantities $\log_{10}\frac{N_{\rm res}}{N}\frac{E_0 d}{\delta S}$, for $E>0$, and $\log_{10}\frac{N_{\rm bound}}{N}\frac{E_0 d}{\delta S}$, for $E<0$, where $N_{\rm res}$ and $N_{\rm bound}$ are the number of resonances and bound states respectively, within each rectangular bin of area $\delta S = \delta E\delta\ln(a_{\rm eff}/d)$ ($\delta E = 0.01E_0$ and $\delta\ln(a_{\rm eff}/d) = 0.007$, for $E>0$, and $\delta E = 0.01E_0$ and $\delta\ln(a_{\rm eff}/d) = 0.004$ $E<0$). (a) No selection is applied to the resonances ($E>0$). As explained in the text, most of the displayed resonances (the ones with a too large width) are not expected to be meaningful. (b) Restricting to $E>0$, only the resonances with a width $\Gamma<\Gamma_{\rm max} = 10^{-6}E_0/\hbar$ are kept in the density of resonances. The value of $\Gamma_{\rm max}$ is essentially infinite with respect to the duration of typical experiments. (c) Only the resonances and bound states corresponding to a small enough participation surface S_p are kept in the density ($S_p^{1/2}/d<9.5$, see Fig.17a and c). (d) Only the resonances and bound states corresponding to a small enough r.m.s. size σ in real space are kept in the density ($\sigma/d<4.2$, see Fig.17b and d).

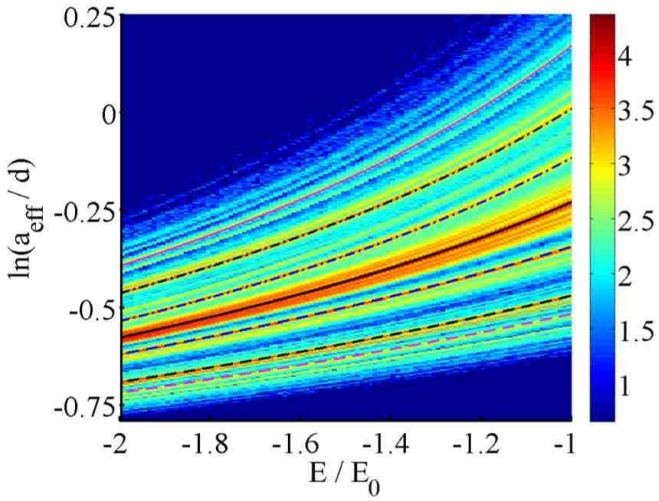

FIG. 15: Zoom of figure 14a, in the region of $E < 0$ (here $\delta E = 0.01E_0$, and $\delta \ln(a_{\rm eff}/d) = 0.003$). On the color map representing the density of states (see caption of Fig.14a), are plotted the energies of bound states of an A atom with one, two or three B atoms, called respectively dimer AB, trimer AB_2, and tetramer AB_3. In particular are plotted the energies of a dimer Eq.(45) (black solid line), of a trimer Eq.(46) with two B atoms separated by a distance $r_{12} = d$ (dashed black and dash-dotted black lines), of a trimer with two B atoms separated by a distance $r_{12} = \sqrt{2}d$ (dashed and dash-dotted blue lines), of a tetramer Eq.(47) with three B atoms separated by distances $r_{13} = r_{23} = d$ and $r_{12} = \sqrt{2}d$ (solid and dashed magenta lines). It is worth noting that the predictions for the energies of such isolated bound states correspond to the higher density lines of the color map plot.

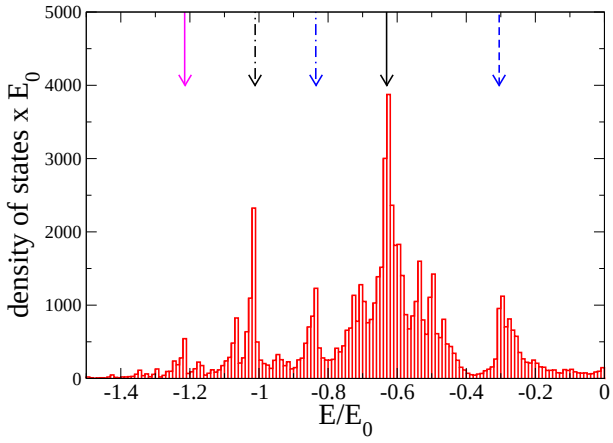

FIG. 16: For the 2D system: density of bound states for a given value of the 2D effective scattering length $a_{\rm eff} = d$. The histogram is the result of the average over 100 random realizations of the scatterers positions in a disk of radius $R = 50d$, and a filling factor $p_{\rm occ} = 1/10$. On average, we find 0.85 bound states per scatterer. As done in Fig.15, we also plot the energies of bound states of an A atom with one, two or three B atoms. The vertical lines with arrows indicate the energies of few body bound states AB_n. Black solid line: energy of a AB dimer Eq.(45), dash-dotted black line: energy of a AB_2 trimer Eq.(46) with two B atoms separated by a distance $r_{12} = d$, dashed and dash-dotted blue lines: energy of AB_2 with two B atoms separated by a distance $r_{12} = \sqrt{2}d$, solid magenta line: energy of the tetramer AB_3 Eq.(47) with three B atoms separated by distances $r_{13} = r_{23} = d$ and $r_{12} = \sqrt{2}d$.

the harmonic confinement in the microtrap.

Acknowledgments

We acknowledge useful discussion with D. Delande. Y.C and M.A. are members of the IFRAF. Numerical calculations have been performed on the IFRAF cluster (the entire work needed several CPU months per core, on 96 Intel Xeon Quadcore processors). M.A. acknowledges financial support from the ERC Project FERLODIM N.228177. D.H. acknowledges financial support from CNRS, UPMC and IFRAF during his stay in Paris.

Appendix A: Monotonic behavior of the eigenvalues of $M(E)$

We show that, for $E = -\frac{\hbar^2 q^2}{2m} < 0$, the eigenvalues $m_i(E)$ of the real symmetric matrix $M(E)$ are monotonic functions of the energy E. This results from the Hellmann-Feynman theorem, and from the fact that the matrix $dM(E)/dE$ is positive in 3D (respectively negative in 2D), so that $dm_i/dE > 0$ in 3D (respectively $dm_i/dE < 0$ in 2D).

Let us start with the 3D case. The idea is to show that, for all $1 \leq i, j \leq N$,

$$\frac{d}{dE} M_{ij}(E) = \frac{2\pi\hbar^2}{m} \langle \mathbf{r}_i | \frac{1}{(E - h_0)^2} | \mathbf{r}_j \rangle, \qquad \text{(A1)}$$

where $h_0 = -\frac{\hbar^2}{2m}\Delta_{\mathbf{r}}^{\rm 3D}$. Since $(E - h_0)^2$ is a positive operator, the positivity of dM/dE readily follows. For $i \neq j$ one has, from Eq.(8), that

$$M_{ij} = -\frac{2\pi\hbar^2}{m} \langle \mathbf{r}_i | \frac{1}{E - h_0} | \mathbf{r}_j \rangle, \qquad \text{(A2)}$$

since $(E - h_0) g_0(\mathbf{r}) = \delta(\mathbf{r})$. Taking the derivative with respect to E gives Eq.(A1). It remains to check that Eq.(A1) also holds for $i = j$ by a direct calculation. On one hand, $M_{ii} = a_{\rm eff}^{-1} - q$ so that $dM_{ii}/dE = m/(\hbar^2 q)$. On the other hand, introducing a closure relation in the plane wave basis, one indeed finds

$$\frac{2\pi\hbar^2}{m} \langle \mathbf{r}_i | \frac{1}{(E - h_0)^2} | \mathbf{r}_i \rangle = \frac{2\pi\hbar^2}{m} \int \frac{d^3k}{(2\pi)^3} \frac{1}{(E - \hbar^2 k^2/2m)^2} = \frac{m}{\hbar^2 q}. \qquad \text{(A3)}$$

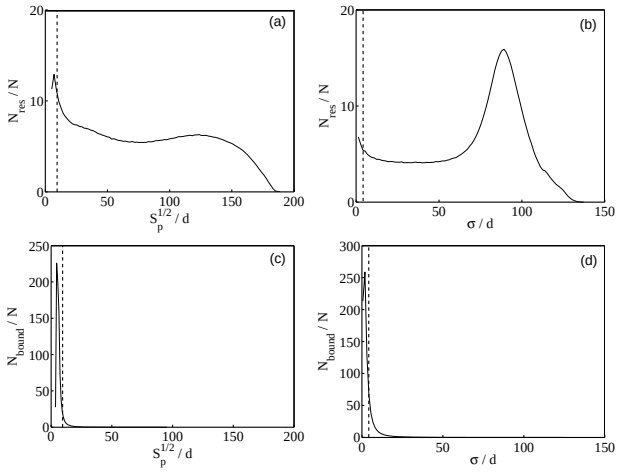

FIG. 17: For the 2D system: For all the resonances with $E_{\rm res}/E_0 \in (0,2)$ and $\ln(a_{\rm eff}/d) \in (-3,3)$, and for all the bound states with $E \in (-2,0)E_0$ and $\ln(a_{\rm eff}/d) \in (-3,3)$, the figures show an histogram giving the number of resonances (in (a) and (b)) and bound states (in (c) and (d)) per scatterer (the number of scatterers is $N = 7 \times 10^3$) as a function of: in (a) and (c), the square root of the participation surface defined in Eq.(44); in (b) and (d), the r.m.s. size in real space defined by the 2D version of Eq.(31). The bin size is $\sim 0.6d$ for (a), $\sim 1.37d$ for (b), $\sim 0.3d$ for (c), and $\sim 1.37d$ for (d). The parameters are the same as in Fig. 14a. The dashed vertical lines are the values $S_{\rm p}^{1/2}/d \simeq 9.5$ and $\sigma/d \simeq 4.2$ [15] used in Fig. 14c and Fig. 14d to select the bound states and resonances that are spatially localized and to filter out the bound states and resonances that are weakly localized.

In 2D, the proof is quite similar. One simply has to show that

$$\frac{d}{dE}M_{ij}(E) = -\frac{\pi\hbar^2}{m}\langle \mathbf{r}_i|\frac{1}{(E-h_0)^2}|\mathbf{r}_j\rangle \qquad \text{(A4)}$$

for all $1 \leq i,j \leq N$, with $h_0 = -\frac{\hbar^2}{2m}\Delta_{\mathbf{r}}^{\rm 2D}$. For $i \neq j$, one has from Eq.(38) that

$$M_{ij} = \frac{\pi\hbar^2}{m}\langle \mathbf{r}_i|\frac{1}{E-h_0}|\mathbf{r}_j\rangle, \qquad \text{(A5)}$$

since $(E-h_0)g_0(\mathbf{r}) = \delta(\mathbf{r})$. For $i=j$, one again performs a direct calculation. First, $dM_{ii}/dE = d\ln q/dE = -1/(2E)$. Second, a closure relation in the plane wave basis indeed gives

$$-\frac{\pi\hbar^2}{m}\langle \mathbf{r}_i|\frac{1}{(E-h_0)^2}|\mathbf{r}_i\rangle = -\frac{\pi\hbar^2}{m}\int\frac{d^2k}{(2\pi)^2}\frac{1}{(E-\hbar^2k^2/2m)^2} = -\frac{1}{2E}. \qquad \text{(A6)}$$

A simple consequence of the monotonic behavior of the eigenvalues m_i, is that the total number of bound states, for a given realization of disorder, is given by the number of positive eigenvalues of $M(E=0)$ in 3D, and by the number of negative eigenvalues of $M(E \to 0^-)$ in 2D.

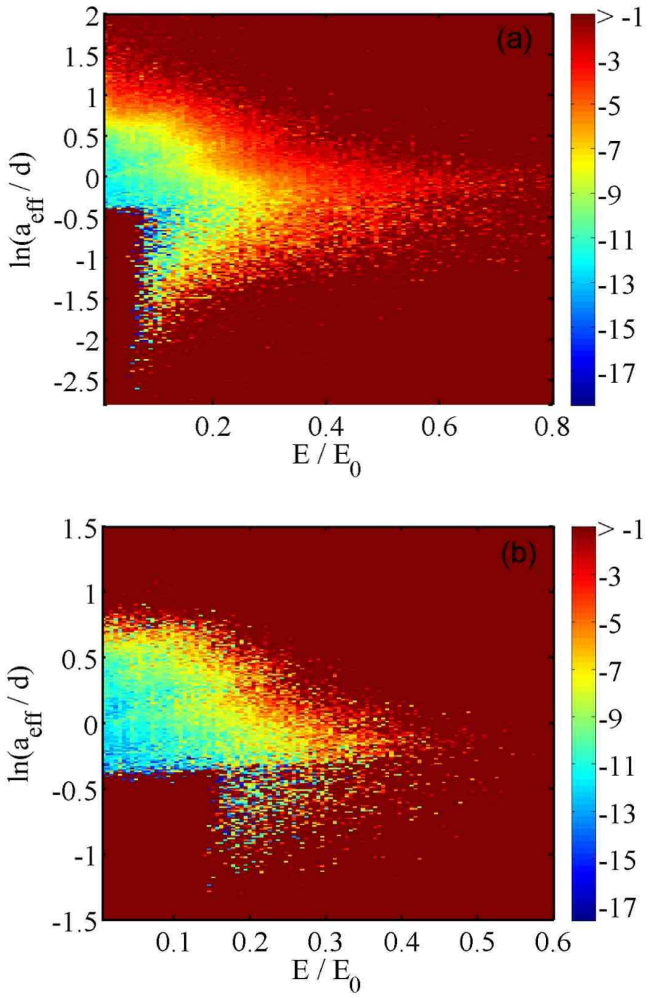

FIG. 18: For the 2D system: Width Γ of the resonances as a function of the energy E and the logarithm of the effective scattering length $\ln(a_{\rm eff}/d)$ [see Eqs. (24) and (27), applied to the eigenvalues $m_i^\infty(E)$ of the matrix M_∞ of Eq.(41)]. The physical parameters are the same as in Fig. 14. The plane $(E, \ln(a_{\rm eff}/d))$ is decomposed in rectangular bins of widths δE and $\delta\ln(a_{\rm eff}/d)$. The color map (see bar on the right) is applied to the quantity $\log_{10}\hbar\langle\Gamma\rangle/E_0$ where $\langle\Gamma\rangle$ is the mean value of Γ for the resonances within a given bin. The resonances are filtered in (a) over the participation volume as in Fig. 14c and in (b) over the r.m.s. size σ as in Fig. 14d. In (a) one has $\delta E = 0.019E_0$ and $\delta\ln(a_{\rm eff}/d) = 0.027$, and in (b) one has $\delta E = 0.011E_0$ and $\delta\ln(a_{\rm eff}/d) = 0.024$.

Appendix B: Matter wave wavefunction in terms of D_i

We restrict here to the three-dimensional case, the generalization to the two-dimensional case being straightforward. Let us consider first a matter wave bound state with eigenenergy $E_0 < 0$. E_0 is a pole of the Green's function $G(\mathbf{r},\mathbf{r}_0)$ defined in Eq.(2), so that, according to Eq.(9), an eigenvalue $m_0(E)$ of the matrix $M(E)$ van-

ishes for $E = E_0$. Since $M(E)$ is real symmetric, its inverse has the spectral decomposition

$$\left[M^{-1}\right]_{ij}(E) = \sum_{n=0}^{N-1} \frac{1}{m_n(E)} D_i^{(n)}(E) D_j^{(n)}(E) \qquad \text{(B1)}$$

where $(D_i^{(n)})_{1\leq i\leq N}$ is the orthonormal eigenvector of $M(E)$ with real components and eigenvalue $m_n(E)$. In particular, $\sum_{i=1}^N (D_i^{(n)})^2 = 1$. When this spectral decomposition is injected in Eq.(9), together with the expansion $m_0(E) = (E - E_0)m'(E_0) + \ldots$, it leads to

$$G(\mathbf{r}, \mathbf{r}_0) \underset{E\to E_0}{\sim} \frac{\psi_0(\mathbf{r})\psi_0(\mathbf{r}_0)}{E - E_0} \qquad \text{(B2)}$$

with

$$\psi_0(\mathbf{r}) = \frac{1}{[m_0'(E_0)]^{1/2}} \sum_{i=1}^{N} D_i^{(0)}(E_0) g_0(\mathbf{r} - \mathbf{r}_i). \qquad \text{(B3)}$$

As it is apparent from Eq.(B2), ψ_0 is the wavefunction of the bound state of energy E_0. Note that $m_0'(E_0)$ is positive according to Appendix A.

Let us consider now a a resonance $z_{\rm res}$ of the system with a complex energy $z_{\rm res}$. Then $z_{\rm res}$ is a pole of the analytic continuation of the Green's function from the upper half-plane to the lower half-plane, so that, according to the corresponding analytic continuation of Eq.(9), an eigenvalue of the matrix $M(z)$ vanishes for $z = z_{\rm res}$. Since $M(z)$ is complex symmetric, if it is diagonalizable its inverse has the spectral decomposition

$$[M^{-1}]_{ij}(z) = \sum_{n=0}^{N-1} \frac{1}{m_n(z)} D_i^{(n)}(z) D_j^{(n)}(z) \qquad \text{(B4)}$$

where $(D_i^{(n)})_{1\leq i\leq N}$ is the right eigenvector of $M(z)$ with complex components and eigenvalue $m_n(z)$, the corresponding left eigenvector is simply its complex conjugate, so that the normalization condition is $\sum_{i=1}^N (D_i^{(n)})^2 = 1$. When this spectral decomposition is injected in the analytic continuation of Eq.(9), together with the expansion $m_0(z) = (z - z_{\rm res})m'(z_{\rm res}) + \ldots$, it leads to

$$G(\mathbf{r}, \mathbf{r}_0) \underset{z\to z_{\rm res}}{\sim} \frac{\psi_0(\mathbf{r})\psi_0(\mathbf{r}_0)}{z - z_{\rm res}} \qquad \text{(B5)}$$

with

$$\psi_0(\mathbf{r}) = \frac{1}{[m_0'(z_{\rm res})]^{1/2}} \sum_{i=1}^{N} D_i^{(0)}(z_{\rm res}) g_0(\mathbf{r} - \mathbf{r}_i). \qquad \text{(B6)}$$

In the limit of an infinitely extended disordered system ψ_0 would correspond to the wavefunction of a localized state of energy $z_{\rm res}$.

[1] P. W. Anderson, Phys. Rev. **109**, 1492 (1958).

[2] J. Billy, V. Josse, Z. Zuo, A. Bernard, B. Hambrecht, P. Lugan, D. Clément, L. Sanchez-Palencia, P. Bouyer, A. Aspect, Nature **453**, 891(2008).

[3] G. Roati, C. D'Errico, L. Fallani, M. Fattori, C. Fort, M. Zaccanti, G. Modugno, M. Modugno, M. Inguscio, Nature **453**, 895 (2008).

[4] J. Chabé, G. Lemarié, B. Grémaud, D. Delande, P. Szriftgiser, and J.C. Garreau, Phys. Rev. Lett. **101**, 255702 (2008).

[5] U. Gavish, and Y. Castin, Phys. Rev. Lett. **95**, 020401 (2005).

[6] P. Massignan, Y. Castin, Phys. Rev. A A **74**, 013616 (2006).

[7] P. Vignolo, Z. Akdeniz, and M.P. Tosi, J. Phys. B **36**, 4535 (2003); B. Horstmann, J.I. Cirac, T. Roscilde, Phys. Rev. A **76**, 043625 (2007); P. Buonsante, F. Massel, V. Penna, A. Vezzani, Phys. Rev. A **79**, 013623 (2009); K.V. Krutitsky, M. Thorwart, R. Egger, R. Graham, Phys. Rev. A **77**, 053609 (2008).

[8] P.W. Anderson, D. J. Thouless, E. Abrahms, D.S. Fisher, Phys. Rev. B **22**, 3519 (1980); P. Erdos and R.C. Herndon, Adv. Phys. **31**, 65 (1982).

[9] An alternative definition of κ, not used in this work, is to consider the logarithm of the angular average of $|t(\mathbf{n})|^2$ rather than the angular average of the logarithm, setting $\kappa_{\rm alt} = -\lim_{R\to+\infty}(2R)^{-1}\langle \ln\langle |t(\mathbf{n})|^2\rangle_{\mathbf{n}}\rangle$ where $\langle\ldots\rangle_{\mathbf{n}}$ is the angular average. From the convexity of the function $x \to -\ln x$ one has $\kappa_{\rm alt} \leq \kappa$. Using the conservation of the flux of probability one can show that

$$\langle |t(\mathbf{n})|^2\rangle_{\mathbf{n}} = 1 - k^{-1}{\rm Im}\sum_{i=1}^{N} D_i s_i \qquad \text{(B7)}$$

with $s_i = (2\pi\hbar^2/m)g_0(\mathbf{r}_i - \mathbf{r}_0)$. To this end one considers the flux of the probability current $\phi_{\rm far}$ through a sphere of arbitrarily large radius and the flux $\phi_{\rm near}$ through a sphere of arbitrarily small radius around the source location $\mathbf{r}_0$. One finds from Eq. (11) that $\phi_{\rm far} = [m/(2\pi\hbar^2)]^2(4\pi\hbar k/m)\langle |t(\mathbf{n})|^2\rangle_{\mathbf{n}}$. Expanding the Green's function close to the source up to order $|\mathbf{r}-\mathbf{r}_0|^0$, one finds $\phi_{\rm near}$ and one obtains Eq. (B7). A practical consequence is that the Lyapunov exponent $\kappa_{\rm alt}$ may be deduced from measurements of the Green's function close to the source.

[10] The energy of the AB_n bound states between an A atom and n B atomic scatterers can be calculated by using equation (23), where the eigenvalues m^∞ of M_∞ can be calculated analytically in the case of $n \leq 4$.

[11] In the limit $p_{\rm occ} \to 0$ the fact that the scatterers positions are distributed on a lattice rather than uniformly in continuous space is expected to be no longer relevant, so that the lattice spacing spacing d drops out of the problem. Three length scales then remain, the mean distance $\rho^{-1/3} = d/p_{\rm occ}^{1/3}$ between scatterers, $1/k$ and $a_{\rm eff}$. From dimensional analysis, $\rho^{1/3}\xi$ is a function of $\rho^{1/3}a_{\rm eff}$ and of $\rho^{-1/3}k$. The minimal achievable ξ is then reached for

values of $a_{\rm eff}$ and $1/k$ proportional to $\rho^{-1/3}$, and scales as $\rho^{-1/3}$. This also motivates the choice of $\rho^{-1/3}$ and $\hbar^2\rho^{2/3}/m$ as units of length and energy, respectively.

[12] B.A. van Tiggelen, A. Lagendijk, A. Tip, G.F. Reiter, Europhys. Lett. **15**, 535 (1991).

[13] As there is no averaging over disorder, the spatial oscillations in the Green's function are not washed out. For values of ξ larger than the ones presented in the figure, that is for ξ getting larger than the lattice constant d, our fitting procedure based on Eq.(10) is no longer appropriate.

[14] G. Lamporesi, J. Catani, G. Barontini, Y. Nishida, M. Inguscio, F. Minardi, Phys. Rev. Lett. **104**, 153202 (2010).

[15] For a uniformly distributed state in the sphere of radius R, one has $V_{\rm p}^{1/3}/R = (4\pi/3)^{1/3} \simeq 1.6$ and $\sigma/R = (3/5)^{1/2} \simeq 0.77$.

[16] This picture is expected for a quadratic matter wave dispersion relation, as considered here. For more complicated dispersion relations, as in the Hubbard model, there may be several mobility edges [18].

[17] P.A. Lee, and T.V. Ramakrishnan, Rev. Mod. Phys. **57**, 287 (1985).

[18] D. Belitz and T. R. Kirkpatrick, Rev. Mod. Phys. **66**, 261 (1994).

[19] F. Evers, and A. D. Mirlin, Rev. Mod. Phys. **80**, 1355 (2008).

[20] The generalized Hellmann-Feynman theorem is $dm_i^\infty(z)/dz = \vec{v}_i{}^* \cdot dM^\infty(z)/dz\vec{u}_i$, where $\vec{u}_i$ and $\vec{v}_i$ are the left and right eigenvectors, respectively, corresponding to the eigenvalue $m_i^\infty(z)$, and normalized as $\vec{v}_i{}^* \cdot \vec{u}_i = 1$. Since $M^\infty(z)$ is complex symmetric, one has $\vec{v}_i = \vec{u}_i{}^*$ so that it suffices to calculate the right eigenvector numerically.

[21] We note the presence of a narrow vertical band of resonances for small values of the energy E in the first energy pixel of Fig.7b. Indeed, for very small values of E (not shown in Fig.7b) an extra-density of long-lived resonances appear, with values of $a_{\rm eff}$ spreading over a large interval (including negative values). Nonetheless, these resonances are not spatially localized, and are eliminated by the filtering used in Fig.7d. These long-lived extended states correspond to $kR \leq 1$, which suggest that they are related to finite size effects.

[22] E. Mandonnet, PhD thesis of Université Paris 6, 2000, online at http://tel.ccsd.cnrs.fr/tel-00011872; F.A. Pinheiro, M. Rusek, A. Orlowski, and B.A. van Tiggelen, Phys. Rev. E **69**, 026605 (2004).

[23] E. Abrahams, P. W. Anderson, D.C. Licciardello, and T.V. Ramakrishnan, Phys. Rev. Lett. **42**, 673 (1979).

[24] L. Pricoupenko, and M. Olshanii, Journal of Physics B **40**, 2065 (2007).

[25] I.S. Gradshteyn, and I.M. Ryzhik, *Table of Integrals, Series, and Products* Fifth edition, (Academic Pres, San Diego, 1994).

[26] A. Lagendijk, B. A. van Tiggelen, Phys. Rep. **270**, 143 (1996); Arnaud Derode, Arnaud Tourin, and Mathias Fink, Phys. Rev. E **64**, 036605 (2001); David Laurent, Olivier Legrand, Patrick Sebbah, Christian Vanneste, and Fabrice Mortessagne, Phys. Rev. Lett. **99**, 253902 (2007).

[27] Y. Castin, J. Phys. IV France **116**, 89-132 (2004).

[28] S. E. Pollack, D. Dries, M. Junker, Y. P. Chen, T. A. Corcovilos, and R. G. Hulet, Phys. Rev. Lett. **102**, 090402 (2009).

[29] The effective scattering length generally differs from the free space scattering length a, due to the effect of the confining potential experienced by the B atoms: It is a function of $a/a_{\rm ho}$ and of the $A-B$ mass ratio, as calculated in [6].

[30] One starts with the exact property that, at an eigenenergy E, the matrix M defined in Eq.(8) has a zero eigenvalue. Setting $E = -\hbar^2q^2/(2m)$, where $q > 0$, q will deviate from $1/a_{\rm eff}$ by an exponentially small amount δq if $a_{\rm eff}\rho^{1/3} \to 0^+$. Then to first order in δq, $E - E_{\rm dim} = -\hbar^2\delta q/(ma_{\rm eff})$. Replacing q with its zeroth order value $1/a_{\rm eff}$ in the off-diagonal terms of $M(E)$, one obtains the eigenvalue problem $(E - E_{\rm dim})D_i = \sum_{j\neq i} t_{\rm trans}(r_{ij})D_j$.

[31] Mathematically, it is possible to construct extended wavefunctions with a finite participation ratio. Restricting for simplicity to the 1D case, we define the unnormalized wavefunction $\psi(x) = \sum_{n=1}^N (n/d)^{1/2}\chi[(x - nd)/(d/n)]$, where d is the spatial period of a 1D lattice, and $\chi(x) = 1$ if $|x| < 1/2$, zero otherwise. None of the N compact support spatial components of ψ overlap, so that $\int_{\mathbb{R}} dx|\psi(x)|^{2k} = \sum_{n=1}^N (n/d)^{k-1}$. The participation length $l_p = (\int_{\mathbb{R}} dx|\psi(x)|^2)^2/(\int_{\mathbb{R}} dx|\psi(x)|^4)$ is thus $l_P = 2Nd/(N+1)$ and has a finite limit $2d$ when $N \to +\infty$. On the contrary, the root mean square size σ diverges as $dN/\sqrt{12}$.

[32] In this regime, one could however imagine a highly improbable realization of disorder where a cavity of radius l with no scatterers exists inside the system. If $\hbar^2/(ml^2) < \rho g_{\rm eff}$ there may be a localized state inside this cavity with $0 < E < \rho g_{\rm eff}$.